Experimental and Analytical Studies on Steel-Reinforced Concrete Composite Members with Bonded Prestressed CFRP tendon under Eccentric Tension

Yu Deng[a], Minhe Shen[a,b], Hexin Zhang[b,*], Peng Zhang[a], Terry Y.P. Yuen[c], Chayanon Hansapinyo[d], Peijun Wang[e], Asif Usmani[f], Afrasyab Khan[g], Jia-Jian Zhao[h]

[a] *School of Civil Engineering and Architecture, Guangxi University of Science and Technology, Liuzhou, China 545006*

[b] *School of Engineering and the Built Environment, Edinburgh Napier University, 10 Colinton Road, Edinburgh, Scotland, UK, EH10 5DT*

[c] *Department of Civil Engineering, National Chiao Tung University, Hsinchu, Taiwan*

[d] *Center of Excellence in Natural Disaster Management, Department of Civil Engineering, Chiang Mai University, Chiang Mai, 50200, Thailand*

[e] *School of Civil Engineering, Shangdong University, Jinan, Shandong Province, China, 250061*

[f] *Department of Building Services Engineering, The Hong Kong Polytechnic University, Hung Hom, Kowloon, Hong Kong*

[g] *Institute of Engineering and Technology, Department of Hydraulics and Hydraulic and Pneumatic Systems, South Ural State University, Lenin Prospect 76, Chelyabinsk, 454080, Russian Federation*

[h] *College of Urban Construction, Zhongkai University of Agriculture and Engineering, Guangzhou, China 510225*

Abstract: This paper reported the very earliest experimental and analytical studies on the bonded Prestressed CFRP tendon enhanced Steel Reinforced Concrete (PSRC) members under eccentric tensile loads. Eight PSRC members were tested under monotonic eccentric tensile loading, and three Steel Reinforced Concrete (SRC) members were simultaneously tested for comparison. The load-deflection relationship, the strain distributions as well as the crack propagation and fracture of concrete were investigated experimentally and analytically. The results demonstrated an improvement in the eccentric tensile capacity of PSRC members upon increasing both the steel and reinforcement ratios, or by reducing the prestress

* Corresponding author

E-mail address: j.zhang@napier.ac.uk (Hexin Zhang)

eccentricity. The results also suggested that an enhancement in the level of prestressing increased can decrease the crack propagation and lateral deflection. Moreover, the validity of the plane-section assumption was confirmed. An analytical model was proposed for predicting the elastic bending capacity of the PSRC members based on the experimental results. The study provided an in-depth understanding of the structural behaviour of PSRC members with bonded prestressed CFRP tendon under the eccentric tension underpinned by the elaborate experimental design and practical analytical model.

Keywords: steel-reinforced concrete composite structure; eccentric tension; bonded prestressed CFRP; prestressed steel-reinforced concrete composite structure.

1. Introduction

Steel-reinforced concrete (SRC) structures have been widely used in construction due to their high load-bearing capacity, excellent ductility, and high energy absorption capacity. Numerous studies have addressed the properties of SRC members under compression, bending, shearing, and combined loading to promote these promising composite structural members [1-5]. Members with tremendous axial tension or eccentric tension have found extensive applications in super high-rise buildings and long-span mega transfer trusses, in which some chord members or columns are potentially subjected to the combined tension forces and bending moments. Under tension, the SRC concrete members will prematurely crack, declining the overall mechanical properties of the structure. This has limited the application of SRC members. Prestressed steel-reinforced concrete composite members could effectively prevent cracks in concrete under tension and have been widely used in engineering

practice due to their high load-bearing capacity, excellent ductility, and large energy absorption capacity.

Research results showed that most of the non-embedded SRC columns are subjected to tensile bending or shear destruction under earthquakes. Therefore, structural measures are required to enhance the sectional capacities of members under eccentric tension. Minami et al. [6] theoretically and experimentally assessed non-embedded SRC columns under eccentric tension. Li et al. [7] concluded that the ideal eccentric tension test data can be found by applying eccentric tension with two hinged supports through studying the performance of concrete-filled steel tubes under eccentric tension. Fu et al. [8-10] also performed experiments and Finite Element Model (FEM) simulations to calculate the ultimate flexural capacity of eccentrically tensioned SRC members with embedded I-shaped steel. Their results showed that the Architecture Institute of Japan (AIJ) Specification and Code for design of composite structures in China resulted in an overly conservative design of SRC members. Based on the test and FEM simulation results, relevant correction formulas were put forward.

Through basic research on SRC components, in 2019, Deng et al. [11] proposed a non-bonded prestressed SRC column and carried out tests to study its mechanical properties under eccentric tension. They found that the prestressed strands can effectively control the formation and intensification of cracks in the eccentric tension column, and in turn, improve the bearing capacity.

With the increasing environmental pollution in recent years, the problem of corrosion of prestressed structures has found increasing importance. The corrosion of steel strands is exacerbated over time, causing a decrease in its structural capacity and service life [12-14]. The application of Carbon Fibre Reinforced Polymer (CFRP) reinforcements [15] could be

an effective solution to eliminate the corrosion problems associated with conventional prestressed SRC. CFRP tendons in nature, possess several favourable properties including a small cross-section, high strength-weight ratio, high corrosion resistance, and outstanding fatigue resistance and it has been widely used in strengthening or repairing damaged or capacity deficient structural elements [16-18]. CFRP tendons are high-strength but lightweight. It is 1.5 times stronger than the steel strand at the same diameter but 1/7 of its weight. It will allow the engineers to adopt a smaller prestressing tendon with many benefits: smaller anchors, smaller duck and less weakening to the overall cross-section strength, etc. CFRP tendons have a very typical elastic behaviour that makes them the perfect candidate for resisting cyclical loading. The application of prestressed CFRP tendons to SRC structures could greatly improve their crack resistance and minimize their deflection under service loads while providing additional rigidity. Extensive works have been carried out on the bending behaviour of prestressed CFRP tendon steel reinforced concrete (PSRC) members [19-22]. So far, only a few investigations [7] have explored the tension-bending behaviour of PSRC members. The PSRC members under eccentric tension are still developing.

This study discusses the behaviour of PSRC members under eccentric tensile loads. A series of experiments were conducted on PSRC eccentric tensile members considering their tensile load eccentricity, the cross-sectional dimension of the steel, the reinforcement ratio, and the prestress level. The failure modes, axial load versus deflection relationships, lateral deflection, and strain responses were emphatically explored. The elastic bending capacity of PSRC members under eccentric tension was also evaluated relative to national codes [23-25].

2. Experimental program

2.1 Specimens

The test samples included eight PSRC members and three SRC members. The main parameters are the tensile load eccentricity, the cross-sectional dimension of the steel, the reinforcement ratio, and the prestress level. Detailed parameters of test specimens are listed in Table 1. The length of all specimens was 2020 mm including the length of the two hinged supports welded at both ends. The sample size is around 1.5-1.75 times smaller than the normal size of the column in buildings and the similar size was also commonly adopted in similar studies on eccentrically compressed concrete columns [26-28]. The cross-section of the concrete sample was a square of 200 mm by 200 mm. The height and width of the I-shaped steel reinforcement were both 50 mm, the thickness of the web was 6 mm, and the flange thickness was 6 mm or 8 mm. Four non-prestressed longitudinal reinforcements with diameters of 6 mm or 10 mm were also arranged in the specimens, and the stirrups with nominal diameters of 8 mm were placed at a 100 mm spacing along the longitudinal section of the concrete. The concrete was prestressed with two post-tensioning CFRP tendons with a nominal diameter of 7 mm at an eccentricity of 50 mm below the centroid on the tension side. To make the tensile forces transmit directly to the steel and non-prestressed longitudinal reinforcements, the tendons were extended from the ends of the concrete members and welded to the endplates using a fillet weld. At the same time, stiffeners were added near the ends to prevent the anchorage zone or end block failure due to the bursting prestress forces. To prevent bond failure between the concrete and I-shaped steel, shear connector studs with a shank diameter of 8 mm and height of 28 mm were welded at a 50 mm spacing on both sides of the steel flange. Details of the test specimens are illustrated in Fig. 1.

2.2. Materials

Pre-mixed concrete was used in this experiment. The concrete properties of 150×150×150 mm^3 concrete cubes were tested according to Chinese Standard GB/T 50152-2012 [29]. The average compressive and tensile strengths were 27.4 MPa and 2.83 MPa respectively, and the elasticity modulus of the concrete was 3.16×10^4 MPa. The CFRP tendons were manufactured by OVM Machinery Co., Ltd, China. The material properties of the steel and reinforcement were supplied by various suppliers. Table 2 listed the measured average values of yield strength, ultimate strength, elastic modulus, and elongation percentage. The ducts for the CFRP tendons were grouted with ZH-1 epoxy resin self-compacting mortar, which could develop excellent CFRP-mortar bonding as demonstrated in previous studies [30].

2.3 Fabrication

The specimens were fabricated in two stages. The first stage involved the casting of eight PSRC with bonded members and three SRC members while the second stage was the post-tensioning of the members with CFRP tendons. The steel member was first formed by welding various steel parts. The steel rebar and a corrugated metal duct with a 32 mm diameter were then fixed to the desired positions on the steel member. To allow the strain gauges (BX120-5AA) to be attached, the rust layer of the steel member and reinforcement were removed and the surface of the test points was flattened and cleaned. The strain gauges were then coated with epoxy resin to protect them from damage. Following that, the pre-mixed concrete was poured in and cured for 28 days, as shown in Fig. 2.

A post-tensioning system was designed to simultaneously prestress two CFRP tendons, resulting in zero prestress loss due to elastic shortening, and ensure no tendon breakage. The CFRP tendons were positioned into ducts and both ends were fixed with extension screws which were securely attached to the reaction steel plate using a nut and washer. In the loaded end, a thin hydraulic oil jack (RSC-10508), a jacking chair, a reaction steel plate, and two sets of barrel anchors were placed. These anchors had different functions; one was placed before the reaction plate, named post-tensioning anchor #1, and the other one was placed after the jacking chair, named working anchor #2. Afterwards, the CFRP tendons were tensioned with the thin type hydraulic oil jack. The post-tensioning set-up is shown in Fig. 3.

The prestressing procedure was as follows: The CFRP tendons were gradually prestressed to five load levels at 20%, 40%, 60%, 80% and 100% of the total prestress force. Upon reaching the desired prestress force, working anchor #2 was fixed, and the jack was unloaded. The specimens were then grouted with epoxy resin mortar and each tendon was monitored for the long-term prestress loss in the tendons as depicted in Fig. 4.

2.4 Test setup and procedure

The eccentrically tensioned elements are very common in the frame structures when the axial tension force and bending moment are applied to a frame element simultaneously. The eccentrical tensioned elements are adopted more frequently in modern buildings due to the constraints of more complex structural design/detailing that accompanying contemporary architectural creations.

The experiments were performed using a 5000 kN hydraulic compression machine, as shown in Fig.5. A new reaction steel frame was fabricated to convert the pressure of a

hydraulic compression machine into tension. The reaction force frame consists of internal and external steel cages. The transformation of pressure and tension were realized by changing the relative positions of the internal and external steel cages. Noteworthy, during the loading process, lateral friction was generated by the bending moment at the end of the specimens, which hindered the sliding of the steel cage and limited the lateral deformation. Therefore, two hinged supports were designed to solve this problem. The eccentric tension was applied through the hinged supports at both ends, where the specimen could rotate around the bearing. The specimens were connected to the reaction steel frame using high-strength bearings.

A combination of the load-controlled and displacement-controlled testing protocol was adopted. A small initial load of 10 kN was applied to the specimens to eliminate slippage at the specimen ends. Prior to the yielding of PSRC members, the specimens were loaded at a 4 kN/min rate and held for 2 minutes at each inspection loading interval for crack inspection. The inspection loading interval was set as 10% of the yield load estimated with the analytical model proposed in Section 4. The loading method was shifted to displacement-controlled with a constant rate of 0.01 mm/s until the stopping criterion described below was met. According to Han et al. [31-33], the tests for members loaded in eccentric compression were stopped when the longitudinal strain reached 40,000 $\mu\varepsilon$ or the axial load of the specimen began to drop. However, the members loaded in eccentric tension would have different behaviour and cannot sustain such a large deformation in the reality. When the longitudinal tensile strain reaches 40,000$\mu\varepsilon$, the structure would have been damaged very severely. Therefore, the stopping criterion was defined as the instance of the applied load began to drop from the peak load (P_u).

An automatic experimental data acquisition system was established to collect the load, strain, and displacement during the test. The tensile load and vertical displacement were measured by the load and displacement sensors of the hydraulic compression machine, respectively. Five extensometers were deployed at equal intervals along the specimen span to monitor deflections. To monitor the response of the strain, 12 strain gauges were attached to the steel surface and longitudinal reinforcements at the mid-height of the specimen. Furthermore, a set of strain gauges were placed along the belly of the concrete side for the strain distribution research at the mid-section, as shown in Fig. 6.

3. Test results and discussions

3.1 Crack propagation and progress of failure

The crack development and failure process of 10 specimens are shown in Fig.7. In the non-prestressed XPL specimen with small eccentricity, multiple transverse cracks occurred on the front surface when the load reached $0.19\,P_u$ with maximum crack widths of 0.11 mm. The existing cracks developed and new cracks appeared with an increase in loading level. When the load reached $0.60\,P_u$, the specimen yielded. Numerous hoop cracks appeared on the concrete surface, the average distance between two cracks on each elevation was 95 mm, but the average crack width on the front elevation was larger than the one on the back elevation. The loading was ceased once the peak load was passed.

For the non-prestressed DPL specimen with large eccentricity, the first transverse cracks appeared on the front surface when the load reached $0.13\,P_u$ with the maximum crack

widths of ~0.15 mm. When the load was increased, the depth of the concrete compression zone gradually enhanced, the transverse cracks extended from the front elevation to the side elevation, and diagonal cracks appeared at both ends of the side surfaces. When the load reached $0.70\,P_u$, the specimen yielded. Several cracks appeared on the front concrete surface and quickly grew wider and the average distance between two cracks on each elevation was 80 mm. The DPL specimen also exhibited a significant bending deformation. It is worth noting that, due to the large eccentricity, there is a compression zone in the middle section of the specimen and no cracks appeared on the backside of the specimen. When the load reached the ultimate load (P_u), the concrete cover on the back elevation was crushed and spalled.

For prestressed specimens with small eccentricity, when the load was approximately $0.3\,P_u$, the first cracks appeared on the front elevation. Compared with the XPL specimen, the emergence of the cracks in PSRC specimens was effectively controlled. The cracks developed slowly with the increase of axial load. When the specimen reached the yield load, multiple cracks occurred in the middle of the concrete. Compared with the specimens without prestressed tendons, they showed fewer cracks and larger crack spacing, which were not less than 110 mm. It is worth noting that the concrete cracks in the typical failure mode were closed again because the prestressed reinforcement had not broken after the specimen was unloaded.

For prestressed specimens with large eccentricity, the prestressed CFRP tendons effectively delayed the occurrence of cracks and the cracking load was about $0.2\,P_u$. By increasing the load, a few cracks appeared more on the front surface. When the specimen reached the yield load, the pressure and tension zones were divided as the crack extension

height was 3/4 of the specimen width. Due to the specimen bending, the cracking of the ZH-1 epoxy resin self-compacting mortar continuously generated sounds. When the load reached P_u, the concrete cover on the back surface was crushed and spalled. Similarly, cracks in the tension zone re-closed after unloading.

In summary, the failure modes of the prestressed CFRP steel-reinforced concrete composite members subject to tensile load were mainly dependent on the load eccentricity. Whether the specimens were prestressed or not, the ultimate failure mode was tensile and flexural. The overall longitudinal deformation of the specimen reached the limit value. The failure mode of all the specimens was ductile, which had obvious characteristics and sufficient reserve capacity for safety. Furthermore, the area of concrete compression was directly correlated with the load eccentricity, i.e. the greater the eccentricity of load, the larger the compression area of concrete.

3.2 Load-carrying capacity

The experimental results of the cracking load, yield load, and ultimate load of the columns are listed in Table 3. For specimens with an eccentricity ratio of 0.2, when the longitudinal reinforcement ratio increased from 0.28% to 0.79%, the yield and ultimate loads of the PSRC specimens showed 17% and 23% enhancement, respectively. When the thickness of the steel flange increased from 6 mm to 8 mm, the yield load and ultimate load of the PSRC specimen also grew by 20% and 30%, respectively. The moment and ultimate bearing capacity of the specimens increased with the raising the reinforcement ratio and steel ratio, but this was limited. With the increase of eccentricity, the influence of the reinforcement

ratio and steel ratio on bearing capacity gradually decreased as by an increase in eccentricity, the bearing capacity was mainly controlled by the concrete and steel skeleton.

Under the same eccentricity, when the prestress level rose from 0 to 0.4, and from 0.4 to 0.6, the cracking load of the specimens with small eccentricity was found to increment by 65% and 23%, respectively. The cracking load of the specimens with larger eccentricity was found to increase by 20% and 10%, respectively. Increasing the prestress level could effectively delay the cracking of the test piece.

3.3 Axial load-displacement curves

Fig. 8 shows the effect of the main parameters on the variations of the axial load by displacement. The characteristics of the P-Δ relationship were similar for all specimens. The typical P-Δ relationship for the PSRC members under eccentric tension consisted of three phases. The first phase was the elastic stage where the curve behaved in an approximately linear manner before the reinforcement yielding. The tangent line of the P-Δ relationship reflected the magnitude of the elastic tensile stiffness which gradually decreased by increasing the load and was not significantly influenced by the main parameters. Stiffness of eccentric load in the specimen was negatively correlated with load eccentricity while positively correlated with reinforcement ratio. The second phase is the elastic-plastic stage in which a reduction was observed in the stiffness and the enhancement function of the prestressed CFRP tendon became more significant. In the third phase (plastic stage), the load increased gradually and the plastic deformation significantly developed because of the

hardening effect. As the axial load of the specimen began to drop, the specimen reached its ultimate tensile strength and was unloaded thereafter.

3.4 Tension versus strain relationships of non-prestressed tendons

The strain response curve of the longitudinal reinforcement and the steel near the tensile load side were plotted based on the measured data of the strain gauge as shown in Fig. 9. During the initial stage of loading, the stress linearly varied with strain with small axial strains of the longitudinal reinforcement and the steel. By increasing the load, the tensile longitudinal reinforcement first entered the yield stage in which the strain of the reinforcement rapidly increased. After this, the specimen was deformed at a much faster rate under the applied load.

For the eccentrically loaded specimen, the longitudinal strain was no longer uniformly distributed around the cross-section, the longitudinal reinforcement strain and the steel strain on the side close to the tensile load were greater than that on the further side from the load. Besides, with increasing the eccentricity, the bending of the specimen got further intensified, while the bearing capacity of the specimen decreased and the influence of various effective factors on the load-strain curve got weaker.

The strain of eccentric tension on the prestressed PSRC specimen was smaller than that of the non-prestressed SRC specimen under the same load. For example, the longitudinal reinforcement strain in the middle of XPL and DPL specimens was 1,023$\mu\varepsilon$ and 1,329$\mu\varepsilon$, respectively. When the load reached 200kN, these values declined to 682$\mu\varepsilon$ and 945$\mu\varepsilon$ for XPL-1 and DPL-1 specimens, respectively. This trend can be attributed to restrained cracking and deformation due to the bonding prestresses, delaying the upward movement of the neutral axis, thus improving the overall force capacity of the section.

3.5 Strain distribution

Fig. 10 depicts the longitudinal strain distribution in the transverse direction under different loading levels. To analyse the cross-sectional strain distribution, and define the load-interval for the test, the loading process was divided into 10 loading stages, in which "n" represents the corresponding loading stage in Fig. 10. When the specimen was loaded in the elastic and elastic-plastic stages, the strain distribution maintained approximately linear along the cross-section and the plane cross-sections remained planar. After entering the plastic stage, the strain distribution of the cross-sections became non-linear, but the cross-section planes still maintained their planar shape.

3.6. Lateral deflection

The lateral deflection curves can be obtained under different load levels by using five equidistant electronic displacement meters, as illustrated in Fig. 11. The electronic displacement meters are manufactured by Liyang City Instrument and Meter Plant in Jiangsu Province in China. The model is YDH-200. They are linear displacement transducers. The measuring range is 200mm, sensitivity 200 $\mu\varepsilon$ /mm, intrinsic error < 5 $\mu\varepsilon$ /mm. Since both ends of the specimen were hinged, the measured lateral deflections were distributed symmetrically about mid-height and shaped as half-sine waves, the lateral deflection of the specimen at the mid-height reached its maximum value. Under the same eccentricity, an increment in the prestress level could effectively control the deflection of the section. When the section entered the yield stage, the control effectiveness gradually decreased. The overall deflection of the PSRC specimen was positively related to the eccentricity while negatively correlated with the prestress level, steel ratio, and longitudinal reinforcement ratio.

4. Analysis of sectional capacities

4.1 General

The experiments highlighted the continuous changes of the position of the neutral axis of the PSRC member with the variation of the load eccentricity. However, the effect of the neutral axis movement on the calculation results was not considered in this formula. When the specimen reached the elastic-plastic stage, two situations may occur in the cross-section: full or partial tension. The elastic bending capacity of the bonded prestressed CFRP tendon steel-reinforced concrete composite members under eccentric tension, which can be obtained through the discussion of the neutral axis distribution.

4.2 Basic assumptions

(1) All the sections conformed to the plane-section assumption;

(2) The effect of the concrete on the tensile area was neglected after cracking;

(3) Perfect bonding existed between the concrete and CFRP tendon, the concrete and reinforcement, and the concrete and steel;

4.3 Criteria for Determining the Level of Eccentricity

According to the definition of SRC eccentric tensile members in the Chinese Code for the design of composite structures (JGJ138-2016), and also considering the previous studies, the criteria for determining the level of eccentricity, large or small, can be defined for the bonded prestressed steel reinforced concrete members: if the axial tensile force acted between the centre of the cross-section and the point of action of the resultant tensile forces from the

reinforcement and I-beam flanges in tension, it can be regarded a small eccentric tension member; otherwise, it is a large eccentric tension member.

4.4. Calculation of prestressed decompression

Due to the bonding effect of the ZH-1 epoxy resin, the decompression load of the prestressed CFRP tendon could be calculated with the assumption of a flat section.

The normal stress on the compression side of concrete caused by the pre-compression can be expressed by:

$$\sigma_{pc}^{'} = -\frac{N_p}{A_n} + \frac{N_p \times e_{pn}}{I_n} y_{1n} \quad (1)$$

The normal stress on the tensile side of concrete caused by the pre-compression stress has the following form:

$$\sigma_{pc} = -\frac{N_p}{A_n} - \frac{N_p \times e_{pn}}{I_n} y_{2n} \quad (2)$$

The stress of prestressed CFRP tendon for zero normal stress on the compression side of concrete after the end of the prestress is as follows:

$$\sigma_{p0} = \left(\sigma_{con} - \sigma_l\right) + \alpha_p \sigma_{pc} \quad (3)$$

where σ_l is the value of prestress losses; σ_{con} is control stress for tensioning; α_p is the ratio of the elastic modulus of CFRP to the elastic modulus of concrete.

Based on the effective cross-sectional area of the prestressed CFRP tendons, when the pre-compressive stress of the specimen is offset, the resultant force of the CFRP tendons can be expressed by:

$$N_{p0} = \sigma_{p0} \times A_p \quad (4)$$

where N_{p0} is the pre-compressive stress of the specimen; A_p is cross-sectional area of the CFRP tendon.

4.5 Calculation of elastic bending capacity

4.5.1 Small eccentric tension member

According to sectional analyses, when the small eccentric tensile specimen reached the yield stage, two positions of the neutral axis can be identified for the PSRC specimen; inside the cross-section and outside the cross-section. In both cases, the reinforcements and steel flanges near the tension side reach the yield load and the reinforcements far from the tension side had not reached the yield load, Therefore, through the assumption of a flat section, the magnitude of strain at different section heights can be solved, as shown in Fig.12.

Case 1: The neutral axis was located inside the test section

The equivalent strain of the concrete section:

$$\frac{\varepsilon_s^{'}}{x-a_s^{'}}=\frac{\varepsilon_{af}^{'}}{a_{af}^{'}-x}=\frac{\varepsilon_p}{h-x-a_p}=\frac{\varepsilon_c}{0.5x}=\frac{\varepsilon_{sy}}{h-x-a_s} \quad (5)$$

where $\varepsilon_s^{'}$ is the strain of the reinforcement far from the tension side; x is the height of the concrete in compression zone; $a_s^{'}$ is the distance between the place which is away from the centroid of the reinforcement on the tension side and the place which is away from the concrete edge on the tension side; $\varepsilon_{af}^{'}$ is the strain of the profile steel flange far from the tension side; $a_{af}^{'}$ is the distance from the place which is away from profile steel flange on tension side to the place which is away from the concrete edge on tension side; ε_p is the strain of the prestressed CFRP tendon; a_p is the distance from the centroid of the prestressed CFRP tendon to the concrete edge on the tension side; ε_c is the strain of the compressive concrete; ε_{sy} is yield strain of the reinforcement; a_s is the distance between the centroid of the reinforcement on tension side and concrete edge on the tension side.

Axial force equilibrium:

$$N'_{y-\min} = 0.5(\varepsilon'_{af} + \varepsilon_{af})E_a(l - a'_{af} + x)t_w + \varepsilon_{af}(h_1 + a'_{af} - x - l)E_a t_w$$

$$+(\varepsilon'_{af} + \varepsilon_{af})E_a(b_1 - t_w)t_f + N_{p0} + \varepsilon_p E_p A_p + \varepsilon_{sy} E_s A_s - \varepsilon'_s E_s A'_s - 0.5\varepsilon_c \cdot 0.8E_c(bx - A'_s) \quad (6)$$

where ε_{af} is the strain of the profile steel flange from the tension side; E_a is the modulus of elasticity of steel; t_w is the width of profile steel web; t_f is the width of profile steel flange; E_p is the modulus of elasticity of the CFRP tendon; E_s is the modulus of elasticity of steel reinforcement; E_c is the modulus of elasticity of concrete; A_s is the total cross-sectional area of reinforcement on the tension side; A'_s is the total cross-sectional area of reinforcement far away from the tension side.

Bending moment equilibrium:

$$M'_{y-\min} = 0.5(\varepsilon'_{af} + \varepsilon_{af})E_a(l - a'_{af} + x)t_w[0.5(l - a'_{af} + x) + a'_{af} - a'_s] +$$

$$\varepsilon_{af}(h_1 + a'_{af} - x - l)E_a t_w[0.5(h_1 + a'_{af} - x - l) + l + x - a_s] + \varepsilon'_{af}E_a(b_1 - t_w)$$

$$t_f(a'_{af} - a_s) + \varepsilon_{af}E_a(b_1 - t_w)t_f(h_1 + a'_{af} - a_s) + (N_{p0} + \varepsilon_p E_p A_p)$$

$$(h - a_p - a'_s) + \varepsilon_{sy}E_s A_s(h - a'_s - a_s) - 0.4\varepsilon_c E_c(bx - A'_s)(0.5x - a'_s) \quad (7)$$

where l is the height of the unyielding steel section; h is the height of the specimens; h_1 is the height of the steel; b_1 is the width of the steel; b is the width of the specimens.

The yield moment and the height of the neutral axis could be calculated by Eqs. (6) and (7).

Case 2: The neutral axis was located outside the test section

The equivalent strain of the concrete section is:

$$\frac{\varepsilon_s^{'}}{a_s^{'}+x}=\frac{\varepsilon_{af}^{'}}{a_{af}+x}=\frac{\varepsilon_p}{h+x-a_p}=\frac{\varepsilon_{sy}}{h+x-a_s} \quad (8)$$

where a_{af} is the distance from the profile steel flange on the tension side to the concrete edge on the same side.

Axial force equilibrium:

$$N_{y-\min}=0.5(\varepsilon_{af}+\varepsilon_{af}^{'})E_a(l-a_{af}^{'}-x)t_w+\varepsilon_{af}E_a(h_1+a_{af}^{'}+x-l)t_w+$$

$$(\varepsilon_{af}+\varepsilon_{af}^{'})E_a(b_1-t_w)t_f+N_{p0}+\varepsilon_pE_pA_p+\varepsilon_s^{'}E_sA_s^{'}+\varepsilon_{sy}E_sA_s \quad (9)$$

Bending moment equilibrium:

$$M_{y-\min}=0.5(\varepsilon_{af}+\varepsilon_{af}^{'})E_a(l-a_{af}^{'}-x)t_w[0.5(l-a_{af}^{'}-x)+a_{af}^{'}-a_s^{'}]+$$

$$\varepsilon_{af}E_a(h_1+a_{af}^{'}+x-l)t_w[0.5(h_1+a_{af}^{'}+x-l)+l-x-a_s]+$$

$$[\varepsilon_{af}(h-a_{af}-a_s^{'})+\varepsilon_{af}^{'}(a_{af}^{'}-a_s^{'})]E_a(b_1-t_w)t_f+(N_{p0}+\varepsilon_pE_pA_p)$$

$$(h-a_p-a_s^{'})+\varepsilon_{sy}E_sA_s(h-a_s-a_s^{'}) \quad (10)$$

The yield moment and the height of the neutral axis could be calculated by Eqs. (9) and (10).

4.5.2. Large eccentric tension member

According to sectional analyses, when the large eccentric tensile specimen reached the yield stage, the position of the neutral axis should be discussed in two cases. Case 1, when the cross-section of the profile is not passed by the neutral axis, the reinforcements on the

tension side reach the yield while the flange of steel, which is far from the tension side, is stretched without yielding. Case 2, when the cross-section of the profile is passed by the neutral axis, the reinforcements on the tension side reach the yield while the flange of steel, which is far from the tension side, is compressed without yielding. Therefore, through the assumption of a flat section, the magnitude of strain at different section heights could be solved, as shown in Fig.13.

Case 1: The neutral axis is outside the steel section.

The equivalent strain of the concrete section is as follows:

$$\frac{\varepsilon_s^{'}}{x-a_s^{'}}=\frac{\varepsilon_a}{0.5h-x}=\frac{\varepsilon_p}{h-x-a_p}=\frac{\varepsilon_c}{0.5x}=\frac{\varepsilon_{sy}}{h-x-a_s} \quad (11)$$

where ε_a is the strain of the total cross-sectional area of steel.

Axial force equilibrium:

$$N_{y-\max}^{'}=\varepsilon_a E_a A_a+N_{p0}+\varepsilon_p E_p A_p+\varepsilon_{sy}E_s A_s-\varepsilon_s^{'}E_s A_s^{'}-0.5\varepsilon_c\cdot 0.8E_c(bx-A_s^{'}) \quad (12)$$

where A_a is the total cross-sectional area of steel.

Bending moment equilibrium:

$$M_{y-\max}^{'}=0.5\varepsilon_a E_a A_a h+(N_{p0}+\varepsilon_p E_p A_p)(h-a_p)+\varepsilon_{sy}E_s A_s(h-a_s)-\varepsilon_s^{'}E_s A_s^{'}a_s^{'}-0.4\varepsilon_c E_c(bx-A_s^{'})(0.5x-a_s^{'}) \quad (13)$$

The yield moment and the height of the neutral axis could be determined by Eqs. (12) and (13).

Case 2: The neutral axis is inside the steel section.

The equivalent strain of the concrete section is as follows:

$$\frac{\varepsilon_{af}^{'}}{x-a_{af}^{'}}=\frac{\varepsilon_{af}}{h-x-a_{af}}=\frac{\varepsilon_{sy}}{h-x-a_{s}} \quad (14)$$

Axial force equilibrium:

$$N_{y-\max}=0.5\varepsilon_{af}E_a(h-x-a_{af})t_w+\varepsilon_{af}E_a(b_1-t_w)t_f+N_{p0}+\varepsilon_pE_pA_p+\varepsilon_{sy}E_sA_s$$

$$-\varepsilon_s^{'}E_sA_s^{'}-\varepsilon_{af}^{'}E_a(b_1-t_w)t_f-0.5\varepsilon_{af}^{'}E_a(x-a_{af}^{'})t_w-0.5\varepsilon_c\cdot 0.8E_c(bx-A_s^{'}) \quad (15)$$

Bending moment equilibrium:

$$M_{y-\max}=0.5\varepsilon_{af}E_aA_{aw}(h-x-a_{af})t_w[0.5(h-x-a_{af})+x-a_s^{'}]+\varepsilon_{af}E_a(b_1-t_w)t_f(h-a_{af}-a_s^{'})$$

$$+(N_{p0}+\varepsilon_pE_pA_p)(h-a_p-a_s^{'})+\varepsilon_{sy}E_sA_s(h-a_s-a_s^{'})-\varepsilon_{af}^{'}E_a(b_1-t_w)t_fa_{af}^{'}-$$

$$0.5\varepsilon_{af}^{'}E_a(x-a_{af}^{'})t_w[0.5(x-a_{af}^{'})+a_{af}^{'}-a_s^{'}]-0.4\varepsilon_cE_c(bx-A_s^{'})(0.5x-a_s^{'}) \quad (16)$$

The yield moment and the height of the neutral axis could be calculated by Eqs. (15) and (16).

4.6. Analysis of experimental and theoretical results

Table 6 lists the experimental and theoretical results of the yield load. As shown in the table, the analytical predictions show a good agreement with the experimental results in general. One can easily notice that the member XPL, i.e., with a small eccentricity setup and zero prestressing, has the largest difference between the analytical and experimental results, this is because in the analytical model with small eccentricity, the yielding force is expected

to be determined by the evenly-yielded yielding capacity of the cross-section of the steel beam, in theoretical calculation. However, it is difficult to achieve this "ideal" condition in a lab test. Hence a lower experimental result. However, the difference between the experimental and analytical results is much smaller for DPL sample with a large eccentricity setup, the yielding occurs when one side of the steel beam reached the yielding point which is much easier to achieve in the lab test. Hence a better agreement between the analytical and theoretical results.

5. Conclusions

The behaviour of the bonded Prestressed CFRP tendon Steel Reinforced Concrete (PSRC) members was experimentally investigated under eccentric tension. Three Steel Reinforced Concrete (SRC) and eight PSRC specimens were fabricated and tested. The impact of the eccentricity of the tensile load, the cross-sectional dimension of the steel, the reinforcement ratio, and the prestressing level was investigated on the structural behaviour. This study also explored crack propagation, the progress of failure, axial-load-deflection relationships, and lateral-deflection-strain responses. The following conclusions were drawn, within the limited scope of this study:

The prestressed force in the CFRP tendon will increase the overall capacity of the member and the ductility of the members with a low eccentricity set up by comparing the P_u/P_y value of XPL-1 and XPL-2 in Table 3. However, opposite observation can be obtained for the members with larger eccentricity (DPL-1 and DPL-2). This is because the prestressed CFRP tendon in the tension zone will help to slow down the crack propagation to ensure a more even stress distribution across the cross-section. It will help to increase the overall yielding capacity more than the ultimate capacity of the member.

The crack width of PSRC specimens decreased upon increasing the prestress applied to the tensile zone of the cross-section. The proposed prestressing technique with the improved consistent bonding design can effectively restrain the cracking and overall lateral displacement of the PSRC specimens.

~~The axial stiffness of the PSRC member was increased by installing a prestressed tendon. The axial stiffness also increased by incrementing the prestress level.(delete)~~

The ultimate tensile capacity and axial stiffness of PSRC members showed a significant enhancement by raising the steel ratio and the reinforcement ratio when comparing the experiment results between XPL-1 and XPL-3, DPL-1 and DPL-3, XPL-1 and XPL-4, DPL-1 and DPL-3, DPL-1 and DPL-4 in Table 3. The ultimate tensile capacity also increased by decrementing the load eccentricity.

The load eccentricity had a significant impact on the structural behaviour of the PSRC members. At high load-eccentricity, limited influences were observed from the longitudinal reinforcement ratio, steel ratio, and the prestress level on the overall structural capacity when comparing the group test results between the members XPL-1 to 4 and DPL-1 to 4 shown in Table 3. The overall structural capacity decreased faster and the lateral displacement incremented more rapidly when the load eccentricity increased.

An analytical model was proposed to predict the bending capacity of the PSRC member within the elastic stage. The analytical results agreed well with the test results except for the non-prestressed member with small eccentricity due to the discrepancy between the theoretical assumption and lab practicality.

Acknowledgements

The authors would like to express their special gratitude to the supports from the National Nature Science Foundation of China (51768008, 52078280), British Council and Ministry of Education, China (UK-China-BRI Countries Education Partnership Initiative), China Postdoctoral Science Foundation Project (2017M613273XB), Nature Science Foundation of Guangxi Zhuang Autonomous Region (2019JJA160137), Key Project of Research and Development of Shandong Province (2019GSF110011), Liuzhou Scientific Research and Technology Development Plan (2017BC40202), Royal Academy of Engineering-Visiting Professor (VP2021\7\12), Royal Academy of Engineering-Industrial Fellowship (IF\192023), 2020 National College Students Innovation and Entrepreneurship Training Program (202010594031), 2020 Guangxi Provincial College Students Innovation and Entrepreneurship Training Program (202010594176, 202010594175), and the Guangxi Provincial Research Enhancement Project for Early to Middle Career Academics (2021KY0363).

References

1. Morino, S., *Recent developments in hybrid structures in Japan—research, design and construction.* Engineering Structures, 1998. **20**(4): p. 336-346.
2. Chen, S. and P. Wu, *Analytical model for predicting axial compressive behavior of steel reinforced concrete column.* Journal of Constructional Steel Research, 2017. **128**: p. 649-660.
3. Begum, M., R.G. Driver, and A.E. Elwi, *Behaviour of partially encased composite columns with high strength concrete.* Engineering Structures, 2013. **56**: p. 1718-1727.
4. Cheng, X., Y. Chen, and D.A. Nethercot, *Experimental study on H-shaped steel beam-columns with large width-thickness ratios under cyclic bending about weak-axis.* Engineering Structures, 2013. **49**: p. 264-274.
5. Lacki, P., A. Derlatka, and P. Kasza, *Comparison of steel-concrete composite column and steel column.* Composite Structures, 2018. **202**: p. 82-88.
6. Minami, K., et al., *Ultimate Strength and Ductility of Bare type Column Base conection in SRC structures under High Axial tention (Part1).* Summaries of technical papers of Annual Meeting Architectural Institute of Japan. C-1, Structures III, Timber structures steel structures steel reinforced concrete structures, 1999(1999): p. 1161-1162.
7. Li, W., L.-H. Han, and T.-M. Chan, *Tensile behaviour of concrete-filled double-skin steel tubular members.* Journal of Constructional Steel Research, 2014. **99**: p. 35-46.
8. Fu, J., et al., *Calculation for ultimate flexural capacity of eccentrically tensioned SRC members with embeded* 工 *-shaped steel.* Journal of Building Structures, 2017. **38**(02): p. 90-98.
9. Chen, X., *Calculation and analysis of the normal section bearing capacity of section steel concrete bending members*. 2015, Chongqing University.
10. Han, W., *The stress performance of eccentric tensile steel concrete beam and the test of crack in the plate are studied*. 2014, Chongqing University.
11. Deng, Y., X. Wu, and P. Zhang, *Experimental study on eccentric tensile properties of prestressed steel reinforced concrete columns.* Journal of Building Structures, 2019. **40**(05): p. 115-123.
12. Vu, N.A., A. Castel, and R. François, *Effect of stress corrosion cracking on stress–strain response of steel wires used in prestressed concrete beams.* Corrosion Science, 2009. **51**(6): p. 1453-1459.
13. Tattoni, S. and F. Stochino, *Collapse of prestressed reinforced concrete jetties: durability and faults analysis.* Case Studies in Engineering Failure Analysis, 2013. **1**(2): p. 131-138.
14. Coronelli, D., et al., *Corroded post-tensioned beams with bonded tendons and wire failure.* Engineering Structures, 2009. **31**(8): p. 1687-1697.
15. Mugahed Amran, Y.H., et al., *Properties and applications of FRP in strengthening RC structures: A review.* Structures, 2018. **16**: p. 208-238.
16. Deng, Y., et al., *Experimental and analytical investigation on flexural behaviour of RC beams strengthened with NSM CFRP prestressed concrete prisms.* Composite Structures, 2021. **257**: p. 113385.
17. Deng, Y., et al., *Experimental study on shear performance of RC beams strengthened with NSM CFRP prestressed concrete prisms.* Engineering Structures, 2021. **235**: p. 112004.

18. Deng, Y., et al., *Crack Resistance of Eccentrically Tensioned Prestressed Steel-Reinforced Concrete Composite Members with CFRP Tendons.* Composite Structures, 2021. Under review.
19. Stoll, F., J. E. Saliba, and L. E. Casper, *Experimental study of CFRP-prestressed high-strength concrete bridge beams.* Composite Structures, 2000. **49**(2): p. 191-200.
20. Dolan, C.W. and D. Swanson, *Development of flexural capacity of a FRP prestressed beam with vertically distributed tendons.* Composites Part B: Engineering, 2002. **33**(1): p. 1-6.
21. Le, T.D., et al., *Performance of precast segmental concrete beams posttensioned with carbon fiber-reinforced polymer (CFRP) tendons.* Composite Structures, 2019. **208**: p. 56-69.
22. Lee, C., S. Shin, and H. Lee, *Balanced Ratio of Concrete Beams Internally Prestressed with Unbonded CFRP Tendons.* International Journal of Concrete Structures and Materials, 2017. **11**(1): p. 1-16.
23. *ANSI/AISC 360-10 Specification for Structural Steel Buildings* 2010, American Institute of Steel Construction.
24. *BS EN 1994-1-1:2004: Eurocode 4, Design of composite steel and concrete structures. General rules and rules for buildings* 2005, European Commission for Standardisation.
25. *JGJ 138-2016: Code for design of composite structures*. 2016, China Academy of Building Research.
26. Oliveira, D.R.C.d., V.L. Branco, and I.I.R. Damasceno, *Eccentrically-compressed reinforced concrete columns strengthened with partial jacketing.* Revista ALCONPAT, 2018. **8**(2): p. 150-162.
27. Lin, G., et al., *Behavior of large-scale FRP-confined rectangular RC columns under eccentric compression.* Engineering Structures, 2020. **216**: p. 110759.
28. Yang, Y.-F., F. Fu, and X.-M. Bie, *Behaviour of rectangular RACFST slender columns under eccentric compression.* Journal of Building Engineering, 2021. **38**: p. 102236.
29. *GB/T 50152-2012: Standard for test method of concrete structures*. 2012, China Academy of Building Research.
30. Bai, Q., *Experimental design method for prestressed concrete beams strengthened with high strength steel wire rope*, in *College of Civil Engineering & Architecture*. 2018, Guangxi University: Naning, Guangxi.
31. Han, L.-H., G.-H. Yao, and Z. Tao, *Performance of concrete-filled thin-walled steel tubes under pure torsion.* Thin-Walled Structures, 2007. **45**(1): p. 24-36.
32. Han, L.-H., S.-H. He, and F.-Y. Liao, *Performance and calculations of concrete filled steel tubes (CFST) under axial tension.* Journal of Constructional Steel Research, 2011. **67**(11): p. 1699-1709.
33. Han, L.-H., W. Li, and R. Bjorhovde, *Developments and advanced applications of concrete-filled steel tubular (CFST) structures: Members.* Journal of Constructional Steel Research, 2014. **100**: p. 211-228.

Nomenclature

Notation and abbreviation

E_c modulus of elasticity of concrete

E_s modulus of elasticity of steel reinforcement

E_a modulus of elasticity of steel

E_p modulus of elasticity of the CFRP tendon

$A_s^{'}$ total cross-sectional area of reinforcement far away from the tension side

A_s total cross-sectional area of reinforcement on the tension side

A_p cross sectional area of the CFRP tendon

A_n net cross-sectional area of prestressed channels

A_a total cross-sectional area of steel

x height of the concrete in compression zone

e eccentricity of normal force

h height of the specimens

h_1 height of the steel

b width of the specimens

b_1 width of the steel

t_f width of profile steel flange

t_w width of profile steel web

y_{1n} distance from the gravity of the net cross section to the edge of the concrete away from the tension side

y_{2n} distance from the gravity of the net cross section to the edge of the concrete on the tension side

e_{pn} distance from the centre of gravity of the net cross section to the resultant point of the steel skeleton and the prestressed tendon

α_p The ratio of the elastic modulus of CFRP to the elastic modulus of concrete

β the coefficient of the rectangle stress block

f_{pk} standard value of prestressed CFRP tendon strength

I_n net moment of inertia

σ_l the value of prestress losses

σ_{con} control stress for tensioning

N_p combined force of prestressed tendons and non-prestressed tendons at the resultant point

N_{p0} the pre-compressive stress of the specimen

$a_s^{'}$ distance between the place which is away from the centroid of the reinforcement on tension side and the place which is away from concrete edge on the tension side

a_s distance between the centroid of the reinforcement on tension side and concrete edge on the tension side

a_p distance from the centroid of the prestressed CFRP tendon to the concrete edge on the tension side

$a_{af}^{'}$ distance from the place which is away from profile steel flange on tension side to the place which is away from concrete edge on tension side

a_{af} distance from the profile steel flange on the tension side to the concrete edge on the same side

$\varepsilon_s^{'}$ strain of the reinforcement far from the tension side

$\varepsilon_{af}^{'}$ strain of the profile steel flange far from the tension side

ε_{af} strain of the profile steel flange from the tension side

ε_a strain of the total cross-sectional area of steel

ε_p strain of the prestressed CFRP tendon

ε_c strain of the compressive concrete

ε_{sy} yield strain of the reinforcement

l height of the unyielding steel section

1

Table.1 Detailed parameters of test specimens

Specimen	Steel section size $b_1 \times h_1 \times t_w \times t_f$ (mm)	Eccentricity e (mm)	Prestress level σ_{con}/f_{pk}	Longitudinal reinforcement		Concrete strength	
				number	diameter (mm)	f_c^0 (MPa)	f_t^0 (MPa)
ZL	50×50×6×6	0	0	4	6	27.4	2.83
XPL	50×50×6×6	20	0	4	6	27.4	2.83
XPL-1	50×50×6×6	20	0.4	4	6	27.4	2.83
XPL-2	50×50×6×6	20	0.6	4	6	27.4	2.83
XPL-3	50×50×6×6	20	0.4	4	10	27.4	2.83
DPL	50×50×6×6	80	0	4	6	27.4	2.83
DPL-1	50×50×6×6	80	0.4	4	6	27.4	2.83
DPL-2	50×50×6×6	80	0.6	4	6	27.4	2.83
DPL-3	50×50×6×6	80	0.4	4	10	27.4	2.83
XPL-4	50×50×6×8	20	0.4	4	6	27.4	2.83
DPL-4	50×50×6×8	80	0.4	4	6	27.4	2.83

1

Table.2 Material mechanical properties index

Material type	Diameter (mm)	Steel grade	Yielding strength f_y (MPa)	Ultimate strength f_u (MPa)	Elastic Modulus E_s (MPa)	Elongation (%)
Reinforcement	6	HRB400	495	608	2×10^5	27.5
	10	HRB400	484	699	2×10^5	25.1
CFRP tendon	7	-	1624	1910	1.54×10^5	-
Steel	-	Q235	347	481	2.05×10^5	28.5
	-	Q345	458	599	2.05×10^5	26.3

2

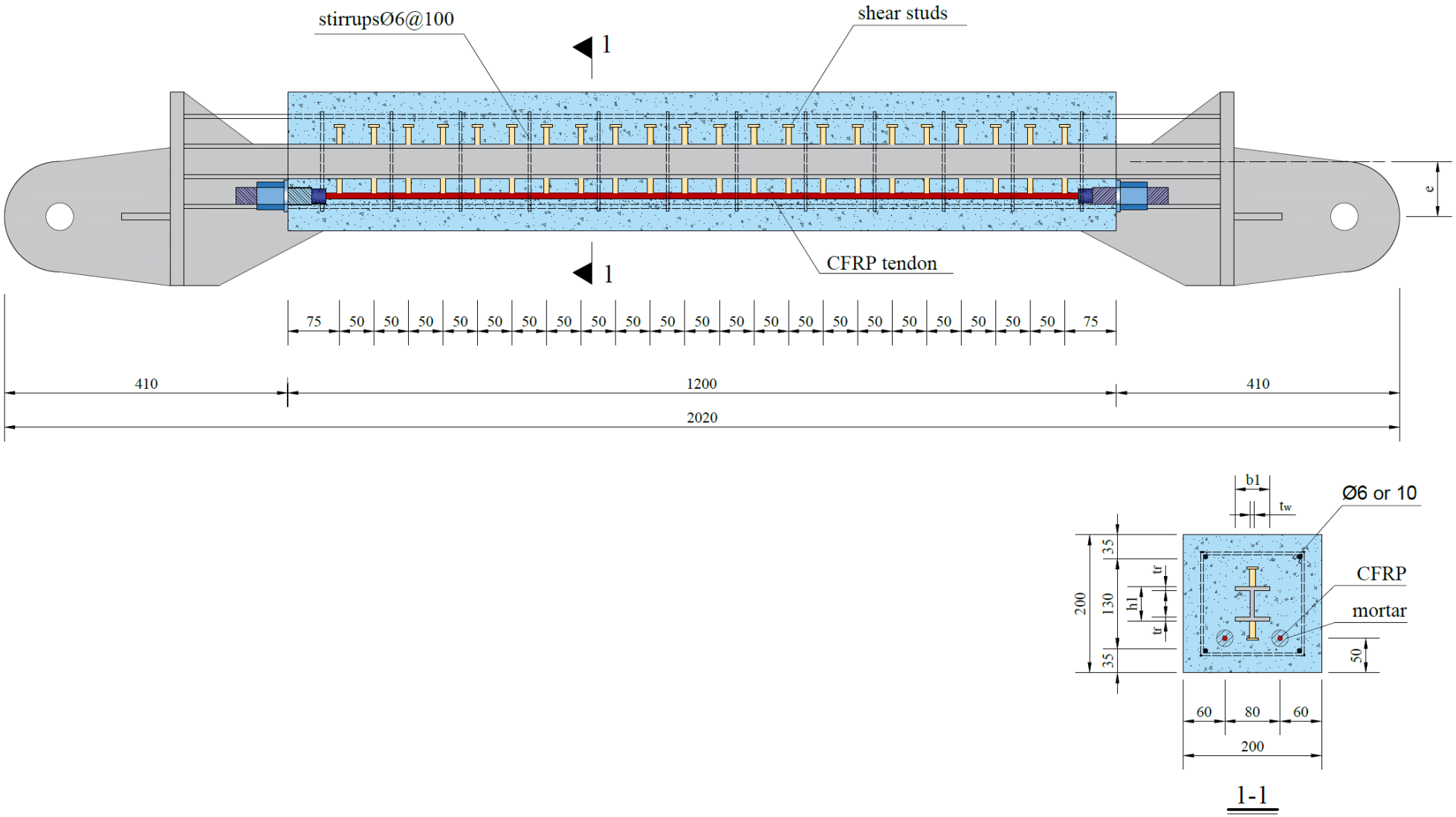

2 Fig.1 Details of test specimens

1

2

3 （a）Fabrication of steel frame section

（b）Layout of formwork

(c) Maintenance of concrete

Fig. 2 Production process

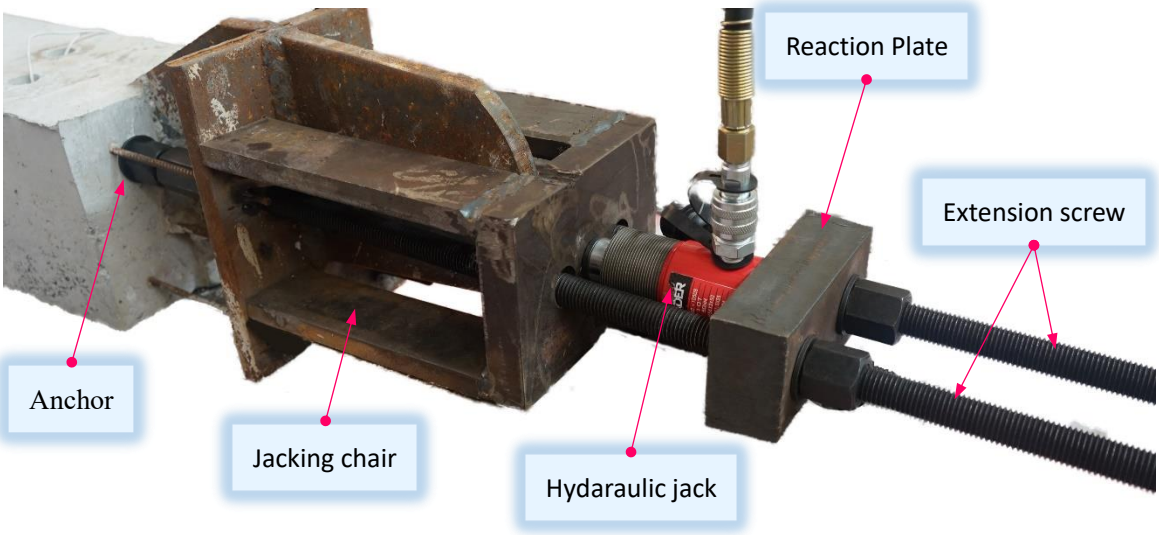

(a) Practicality picture of the post-tension hydraulic device

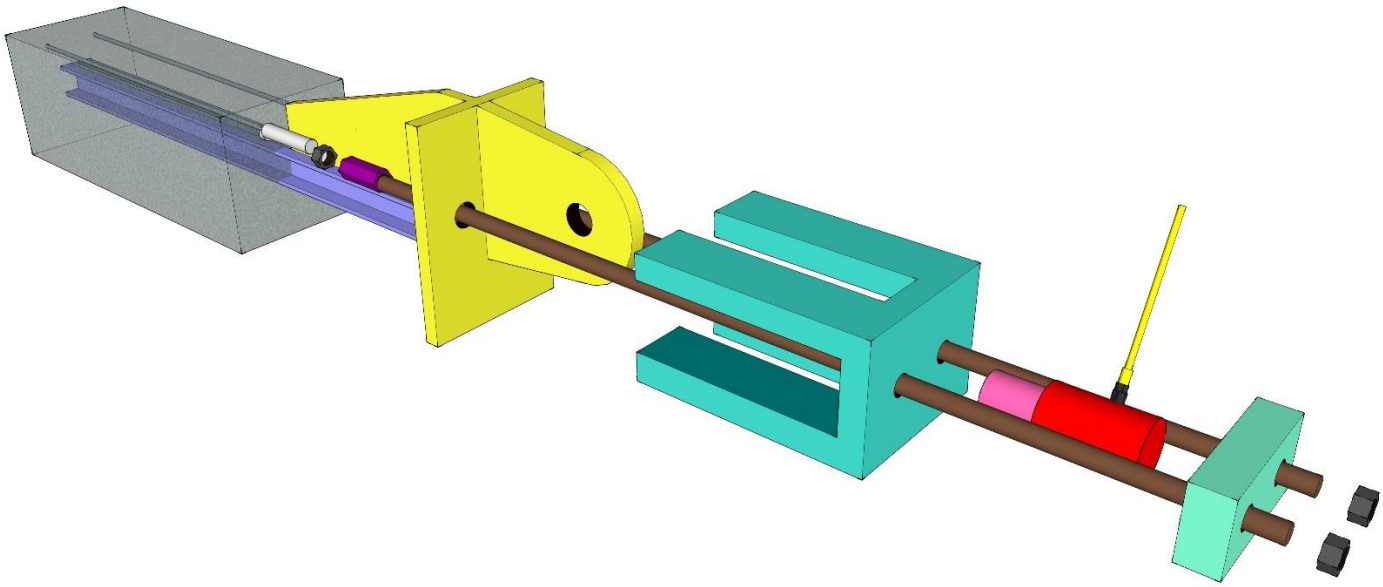

(b) Exploded view of the post-tension hydraulic device

Fig.3 The post-tension hydraulic device

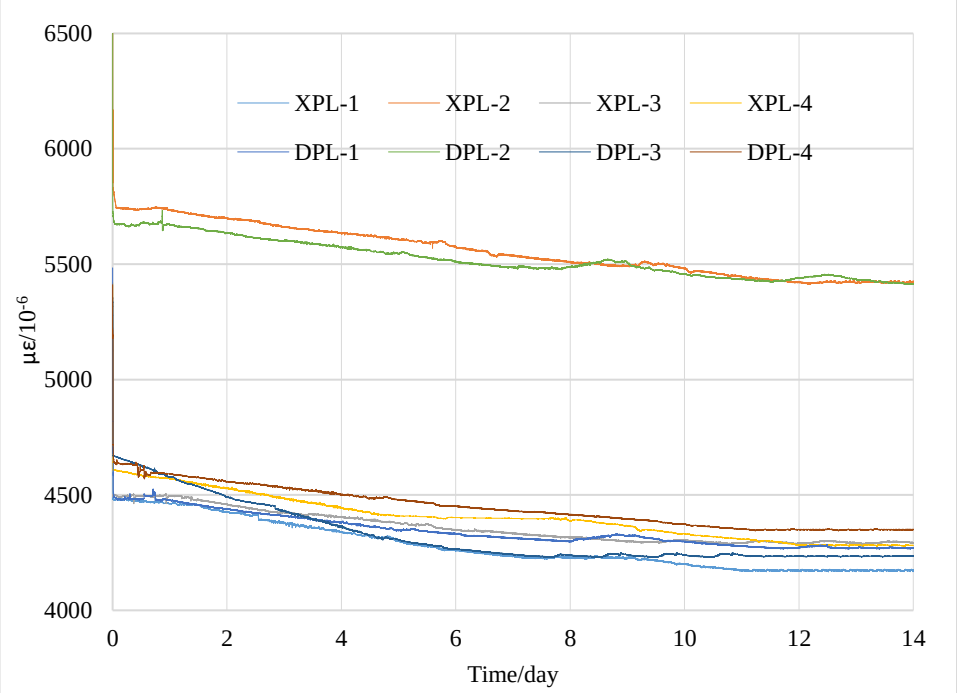

Fig.4 Prestress loss relationship curve

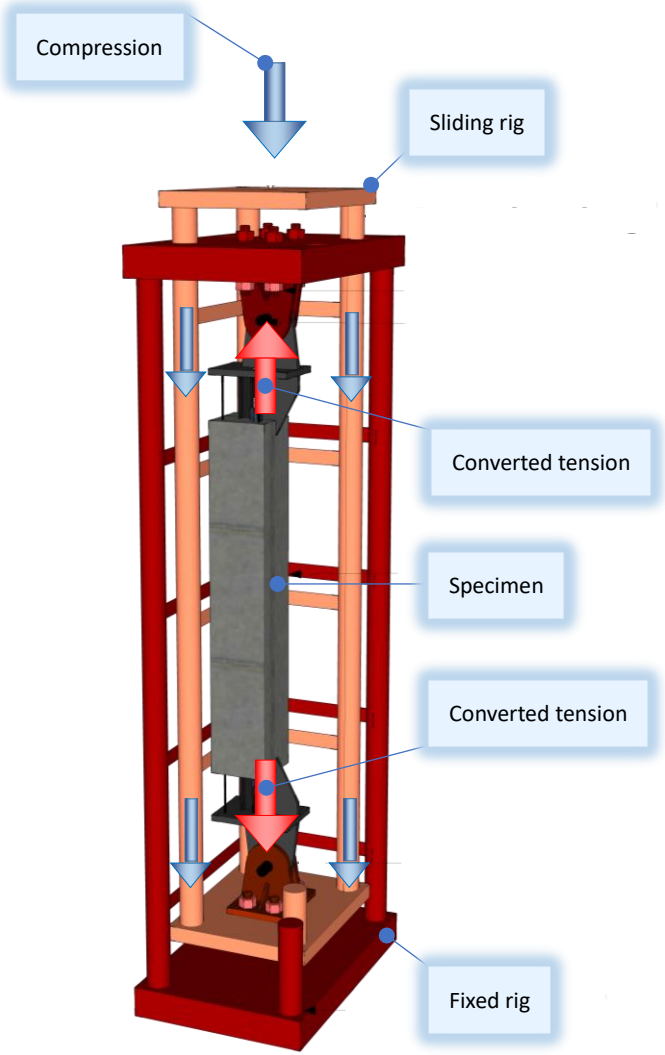

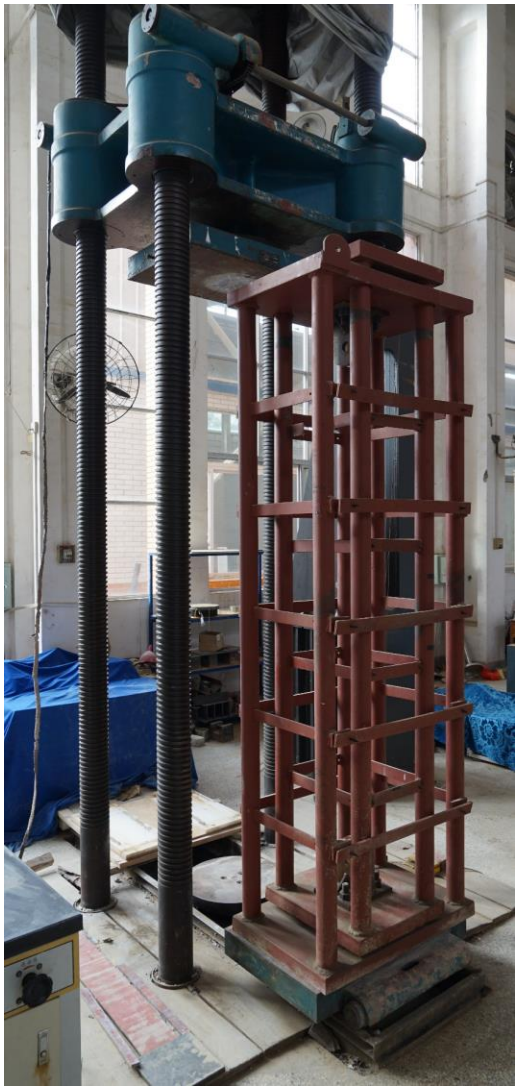

2 (a） Test rig (b) Schematic view of compression to tension test rig (c) Practicality picture

3 Fig.5 Test setup

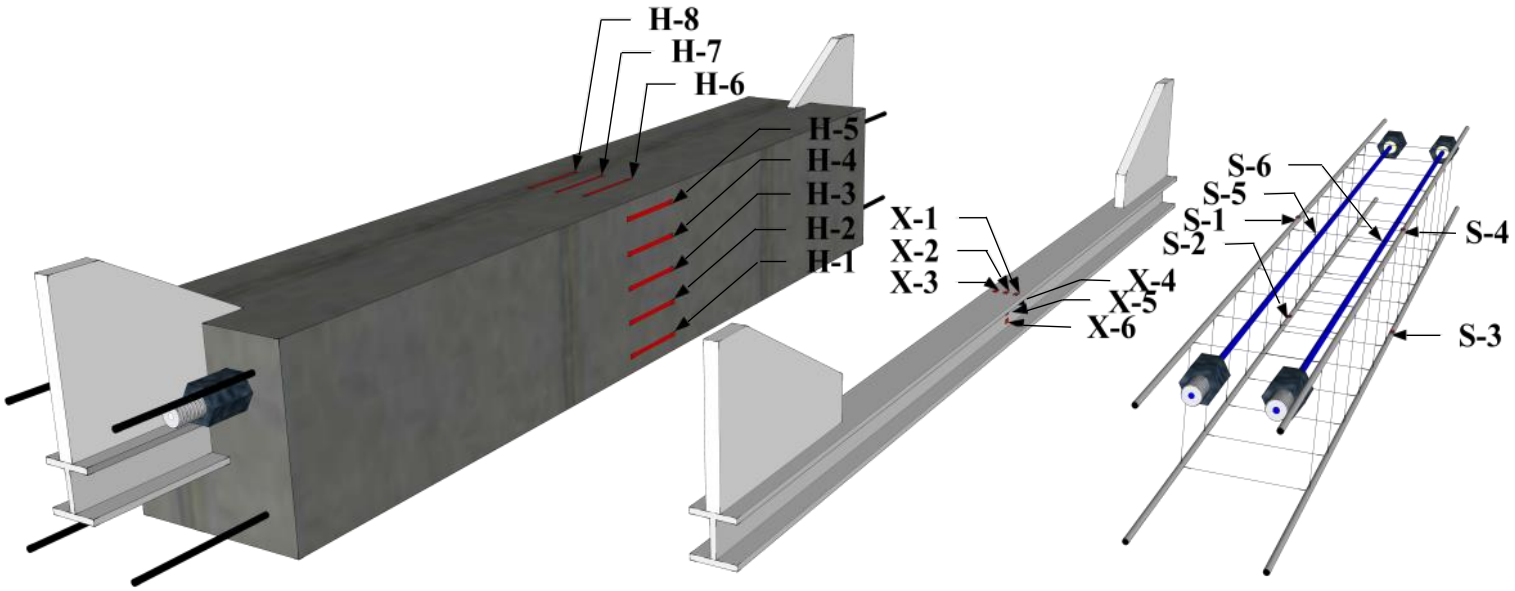

1

2 Fig.6 Strain gauge layout

(a) XPL (b) DPL (c) XPL-1 (d) XPL-2 (e) XPL-3 (f) XPL-4 (g) DPL-1 (h) DPL-2 (i) DPL-3 (j) DPL-4

Fig.7 Cracking and failure pattern of lateral elevation

1

1

Table.3 Load-carrying capacity of specimens

Specimen	P_{cr} /kN	P_y /kN	P_u /kN	P_{cr}/P_y	P_u/P_y
ZL	97	307	460	0.31	1.50
XPL	88	267	443	0.32	1.65
XPL-1	145	343	510	0.42	1.49
XPL-2	178	332	528	0.54	1.59
XPL-3	155	402	629	0.38	1.56
DPL	47	248	354	0.19	1.42
DPL-1	76	300	419	0.25	1.40
DPL-2	102	319	430	0.32	1.35
DPL-3	81	332	455	0.24	1.37
XPL-4	145	374	599	0.39	1.60
DPL-4	79	341	437	0.23	1.28

2

3

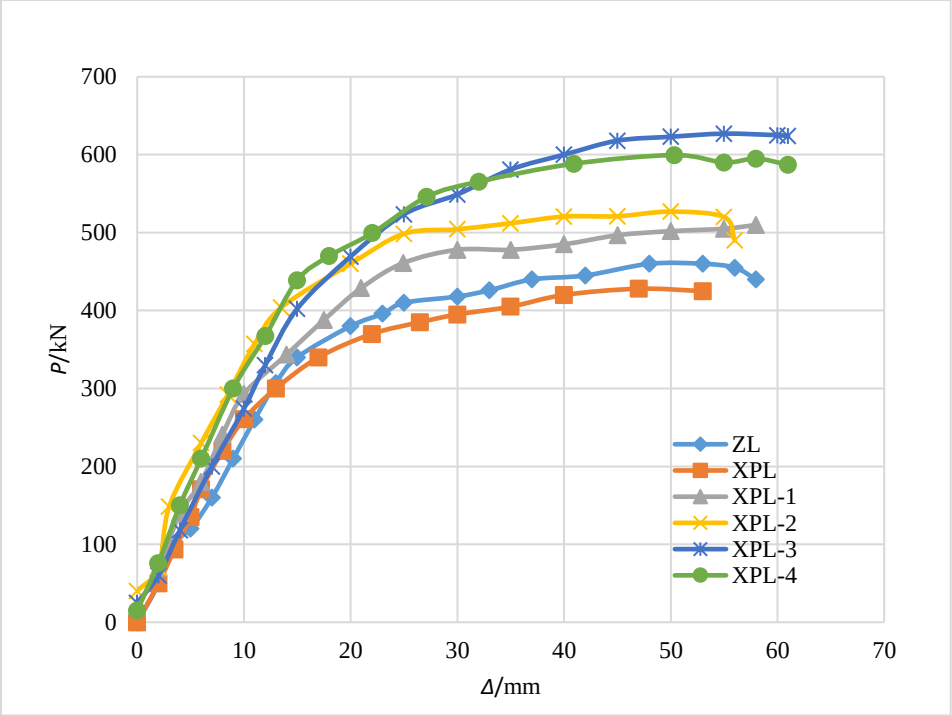

(a) Specimens with *e* of 20

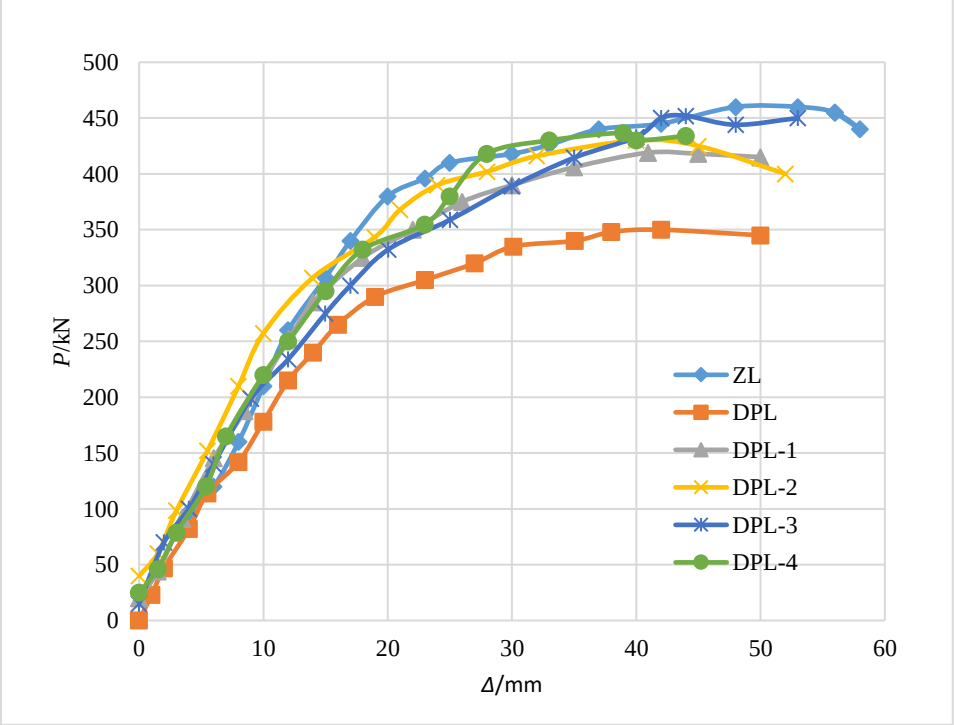

(b) Specimens with *e* of 80

Fig.8 Load-longitudinal displacement curve

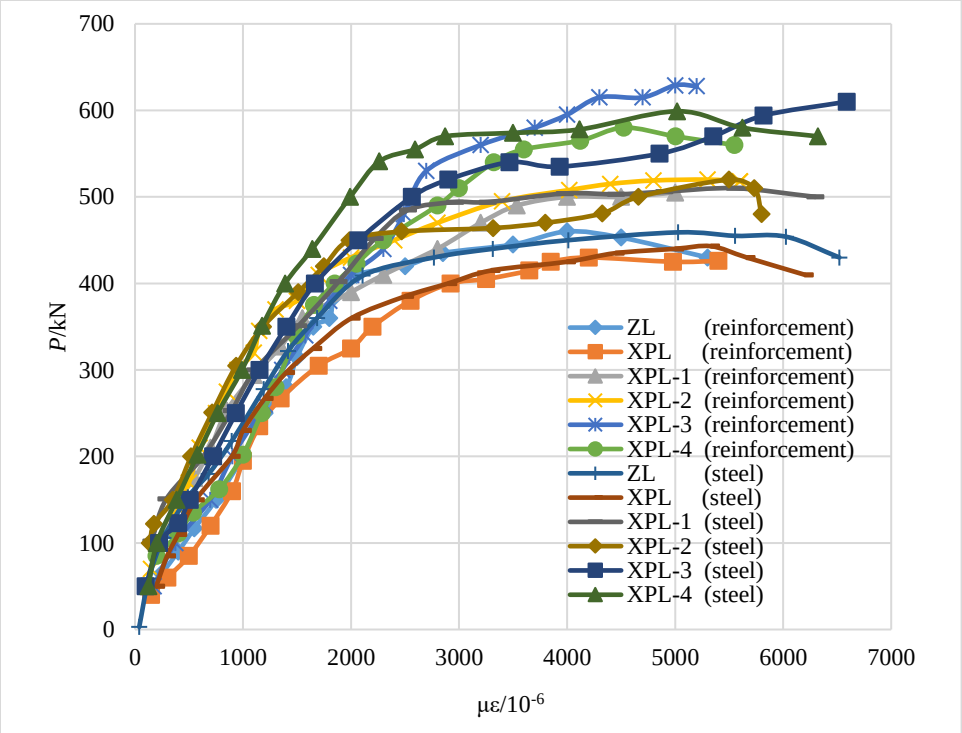

(a) Specimens with *e* of 20

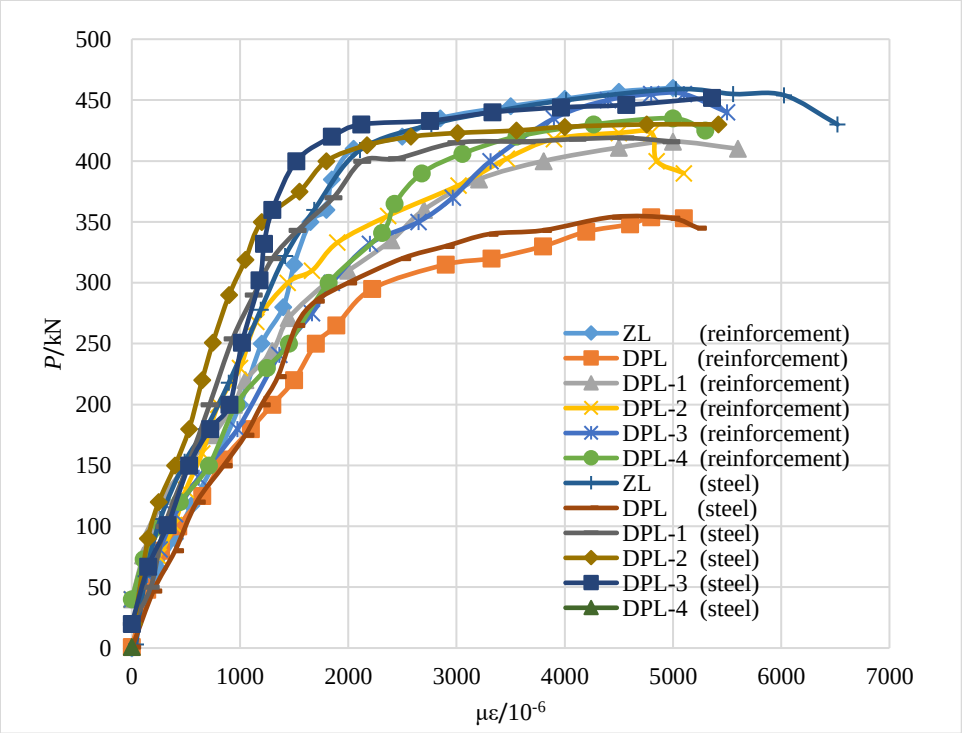

(a) Specimens with *e* of 80

Fig.9 Load-strain curve of steel

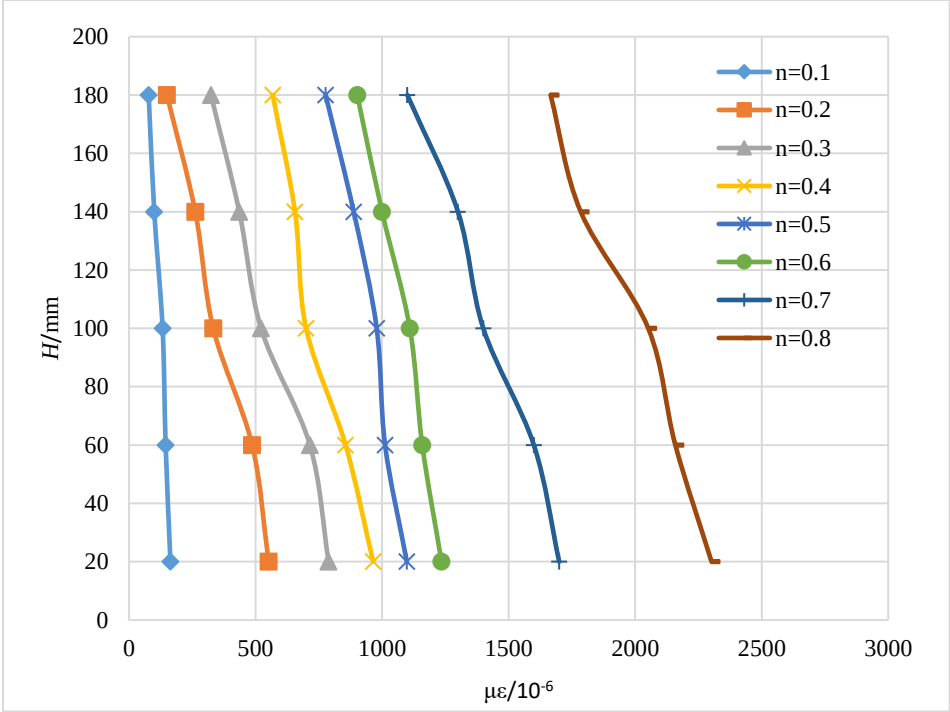
200
180
160
140
120
100
80
60
40
20
0
H/mm
0
500
1000
1500
2000
2500
3000
με/10-6
n=0.1
n=0.2
n=0.3
n=0.4
n=0.5
n=0.6
n=0.7
n=0.8

(a) XPL

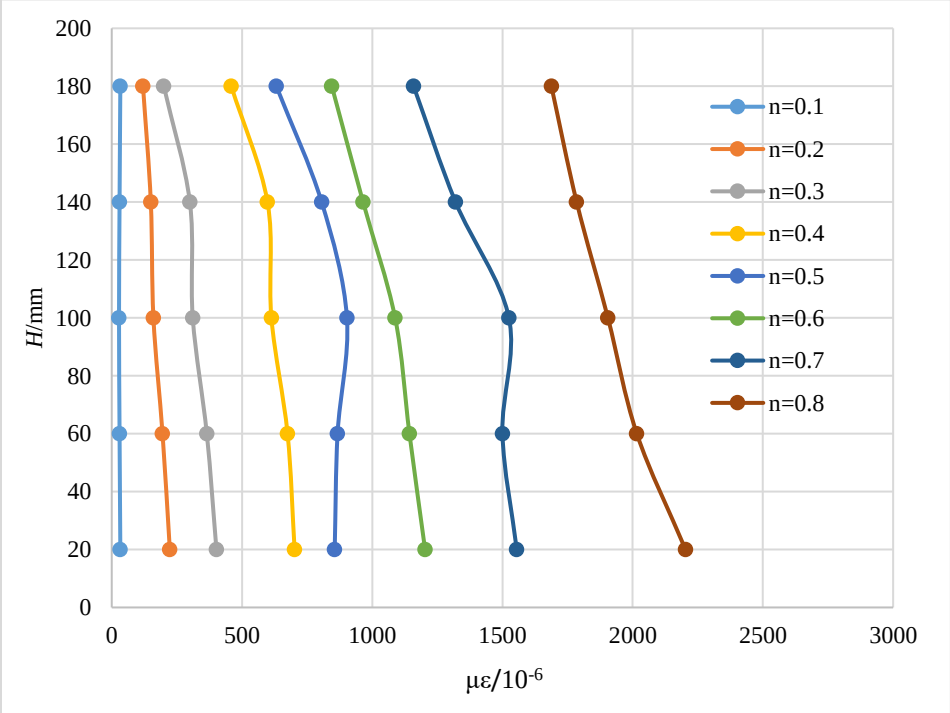
200
180
160
140
120
100
80
60
40
20
0
H/mm
0
500
1000
1500
2000
2500
3000
με/10-6
n=0.1
n=0.2
n=0.3
n=0.4
n=0.5
n=0.6
n=0.7
n=0.8

(b) XPL-1

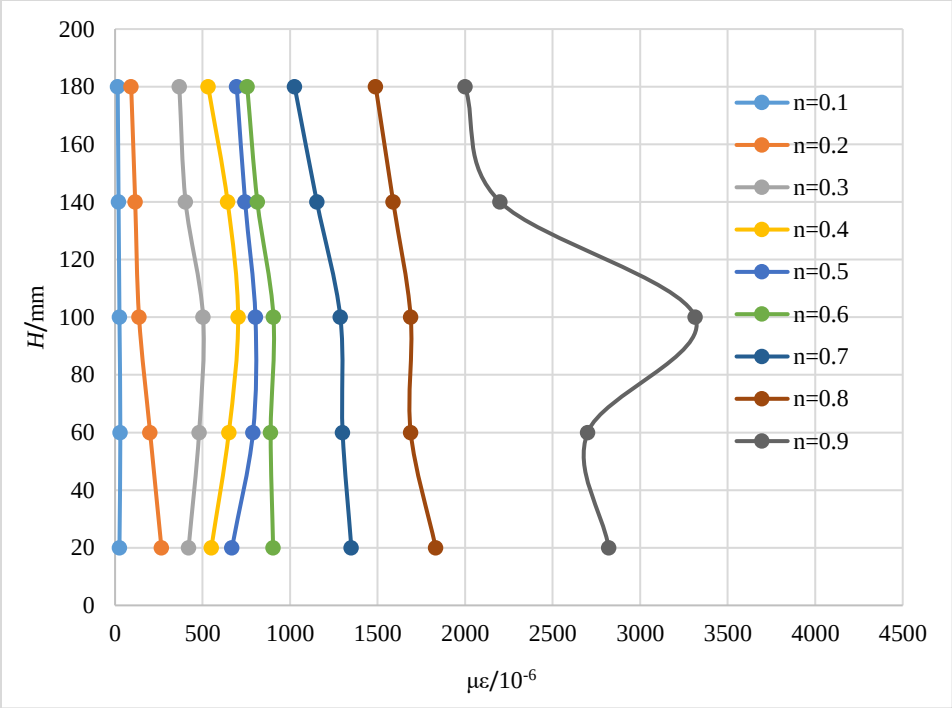
200
180
160
140
120
100
80
60
40
20
0
H/mm
0
500
1000
1500
2000
2500
3000
3500
4000
4500
με/10-6
n=0.1
n=0.2
n=0.3
n=0.4
n=0.5
n=0.6
n=0.7
n=0.8
n=0.9

(c) XPL-2

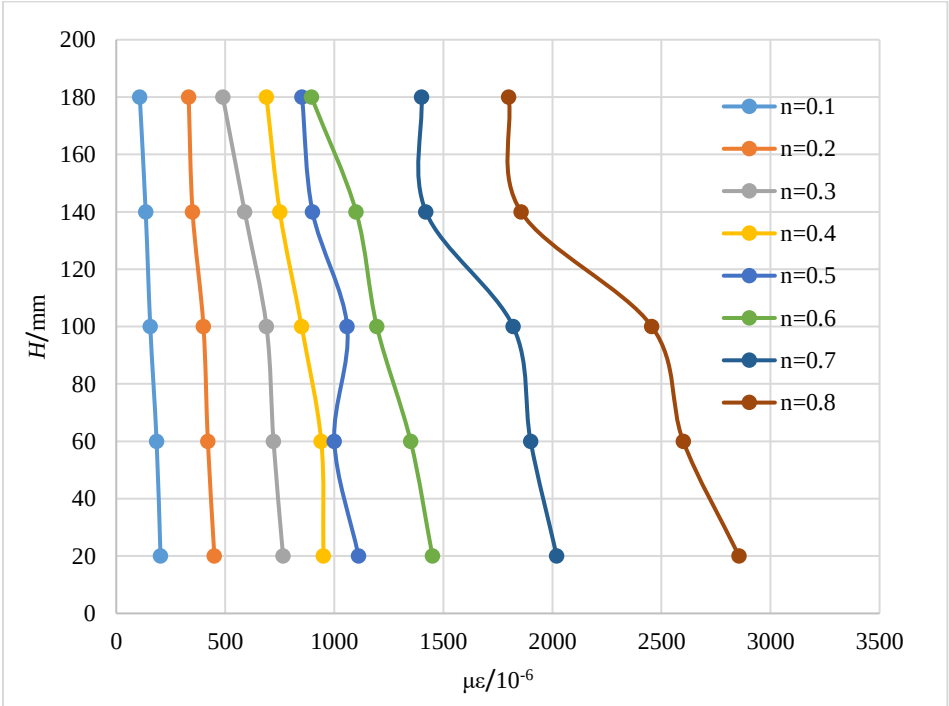
200
180
160
140
120
100
80
60
40
20
0
H/mm
0
500
1000
1500
2000
2500
3000
3500
με/10-6
n=0.1
n=0.2
n=0.3
n=0.4
n=0.5
n=0.6
n=0.7
n=0.8

(d) XPL-3

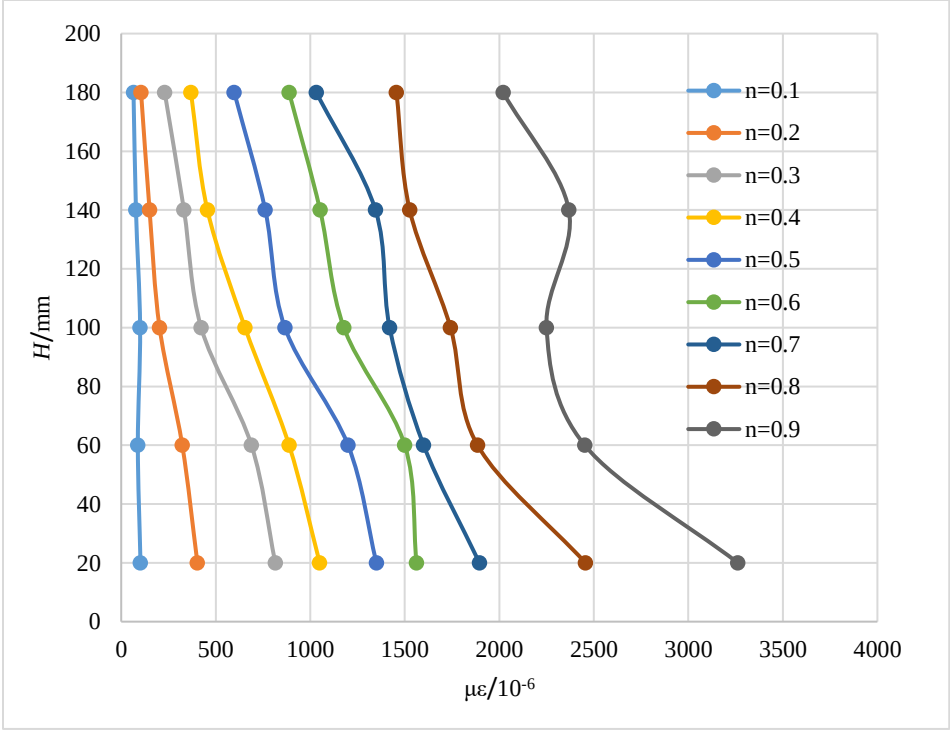
200
180
160
140
120
100
80
60
40
20
0
H/mm
0
500
1000
1500
2000
2500
3000
3500
4000
με/10-6
n=0.1
n=0.2
n=0.3
n=0.4
n=0.5
n=0.6
n=0.7
n=0.8
n=0.9

(e) XPL-4

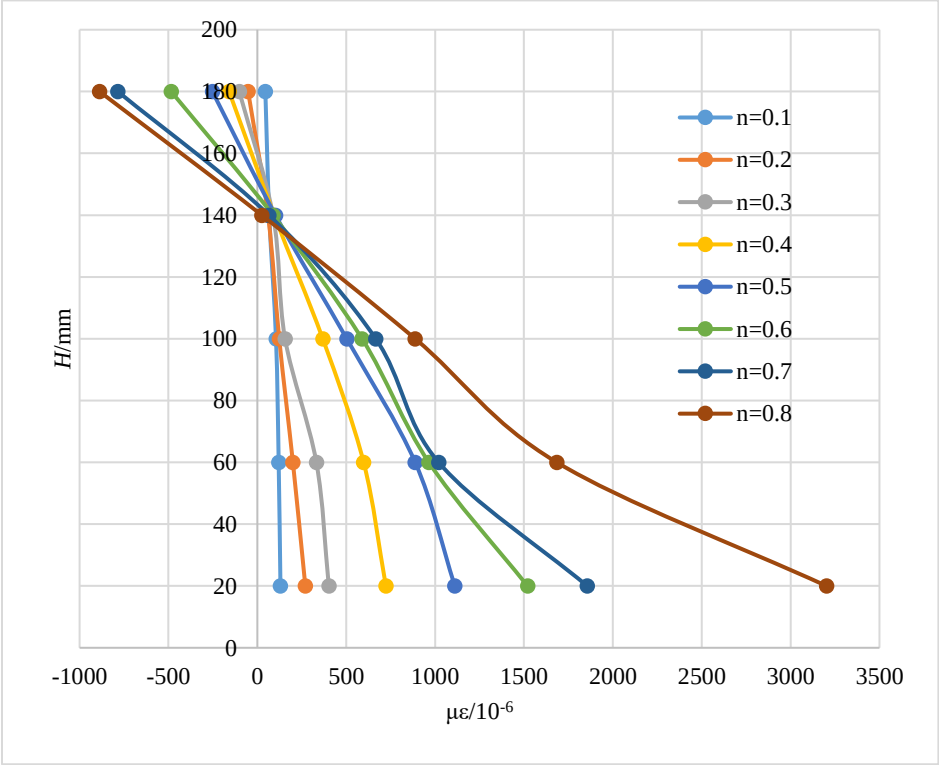
200
180
160
140
120
100
80
60
40
20
0
H/mm
-1000
-500
0
500
1000
1500
2000
2500
3000
3500
με/10-6
n=0.1
n=0.2
n=0.3
n=0.4
n=0.5
n=0.6
n=0.7
n=0.8

(f) DPL

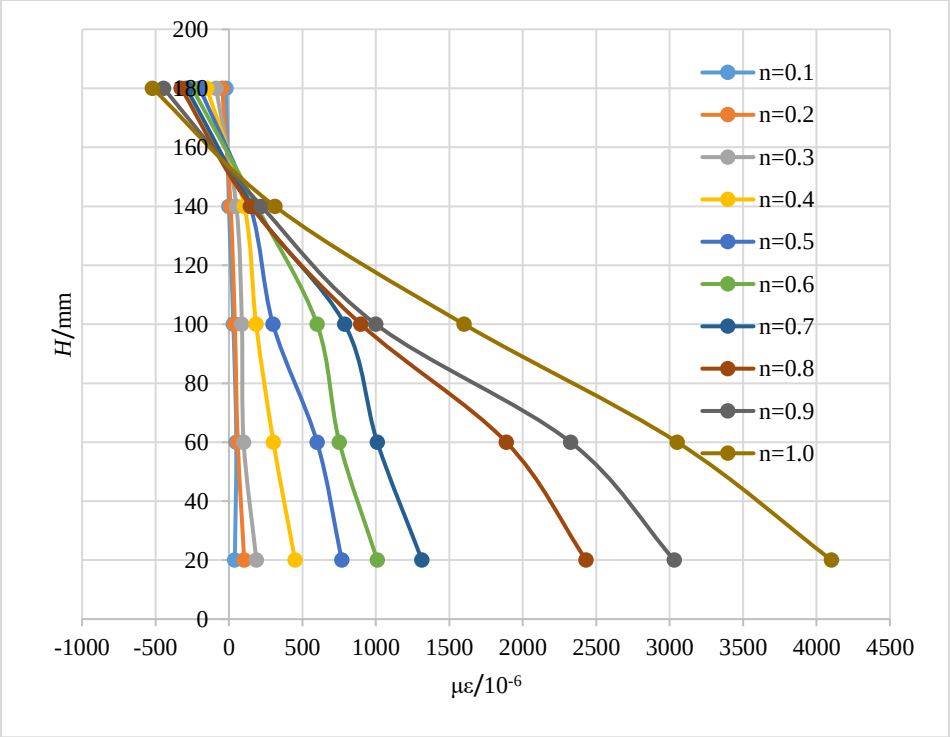
200
180
160
140
120
100
80
60
40
20
0
H/mm
-1000
-500
0
500
1000
1500
2000
2500
3000
3500
4000
4500
με/10-6
n=0.1
n=0.2
n=0.3
n=0.4
n=0.5
n=0.6
n=0.7
n=0.8
n=0.9
n=1.0

(f) DPL-1

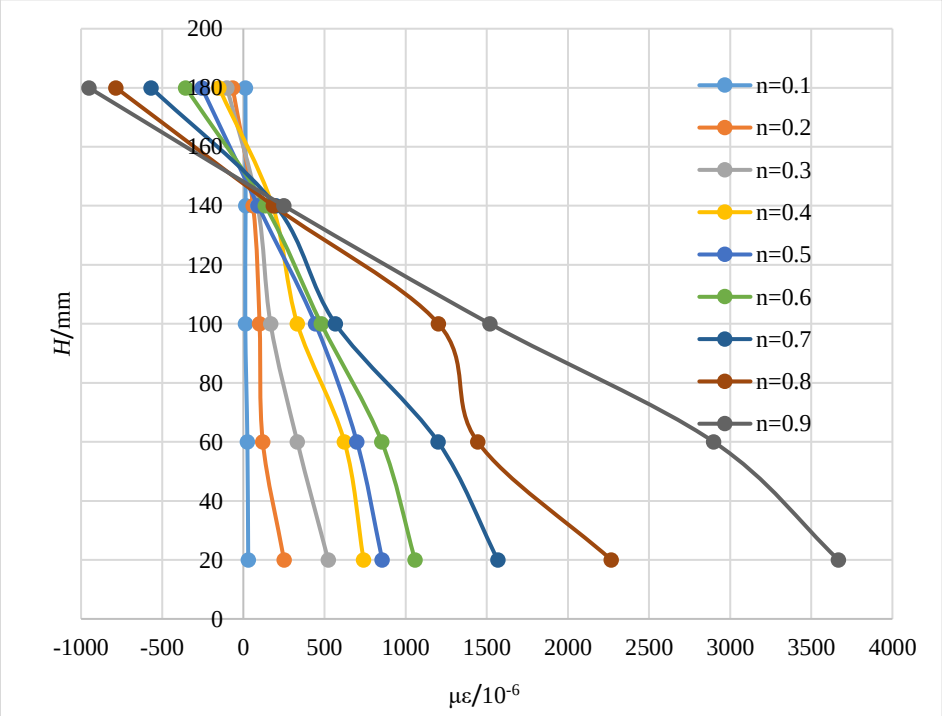
200
180
160
140
120
100
80
60
40
20
0
H/mm
-1000
-500
0
500
1000
1500
2000
2500
3000
3500
4000
με/10-6
n=0.1
n=0.2
n=0.3
n=0.4
n=0.5
n=0.6
n=0.7
n=0.8
n=0.9

(g) DPL-2

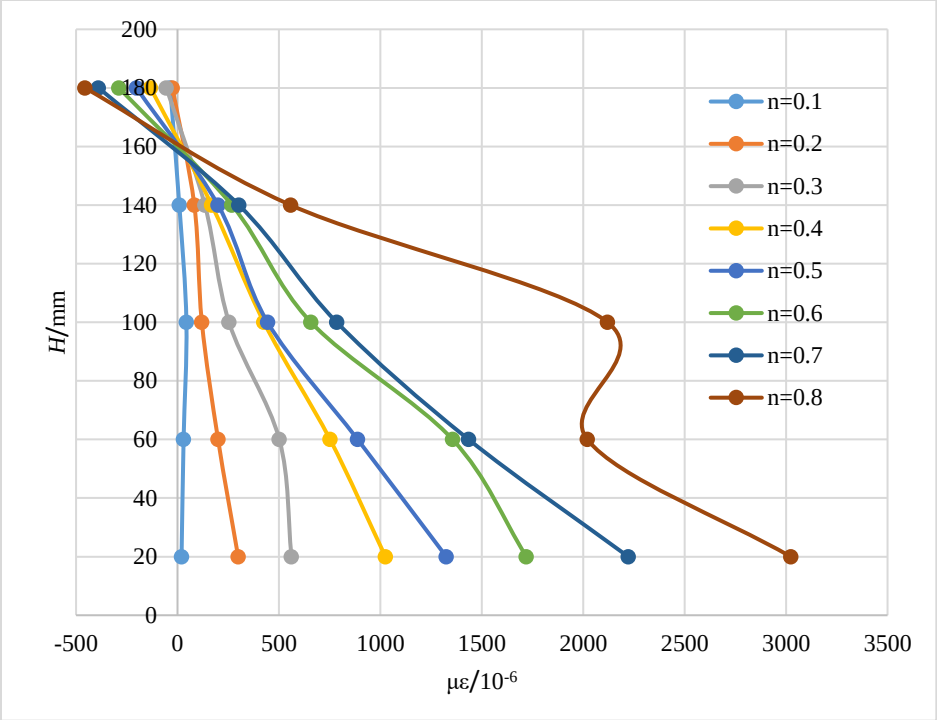

(h) DPL-3

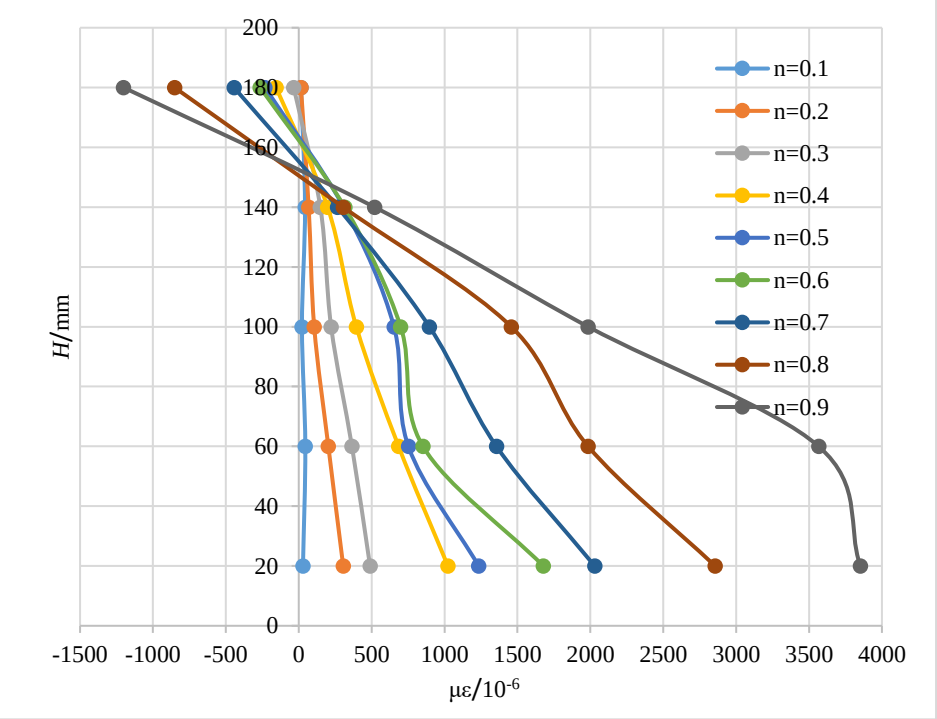

(i) DPL-4

Fig.10 Cross-section strain distribution

1

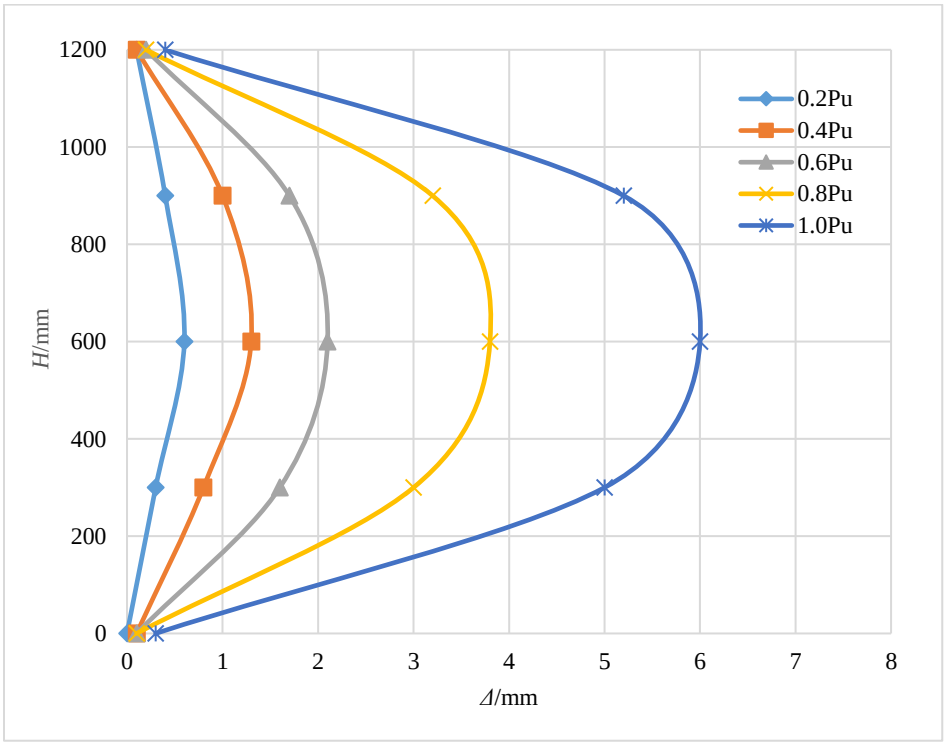

2

3 (a) XPL

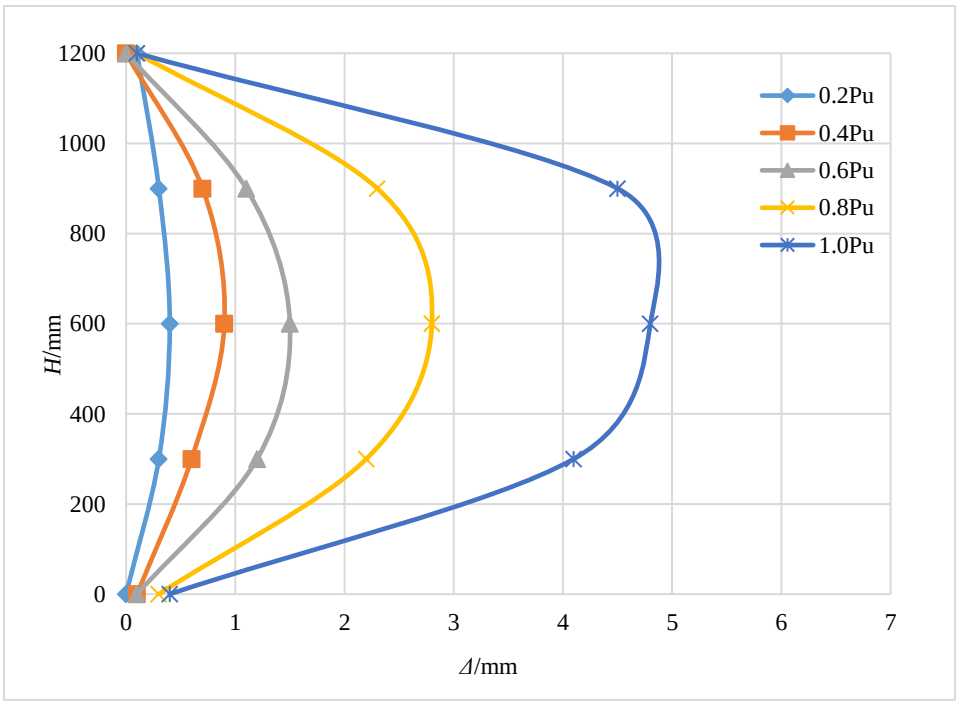

4

5 (b) XPL-1

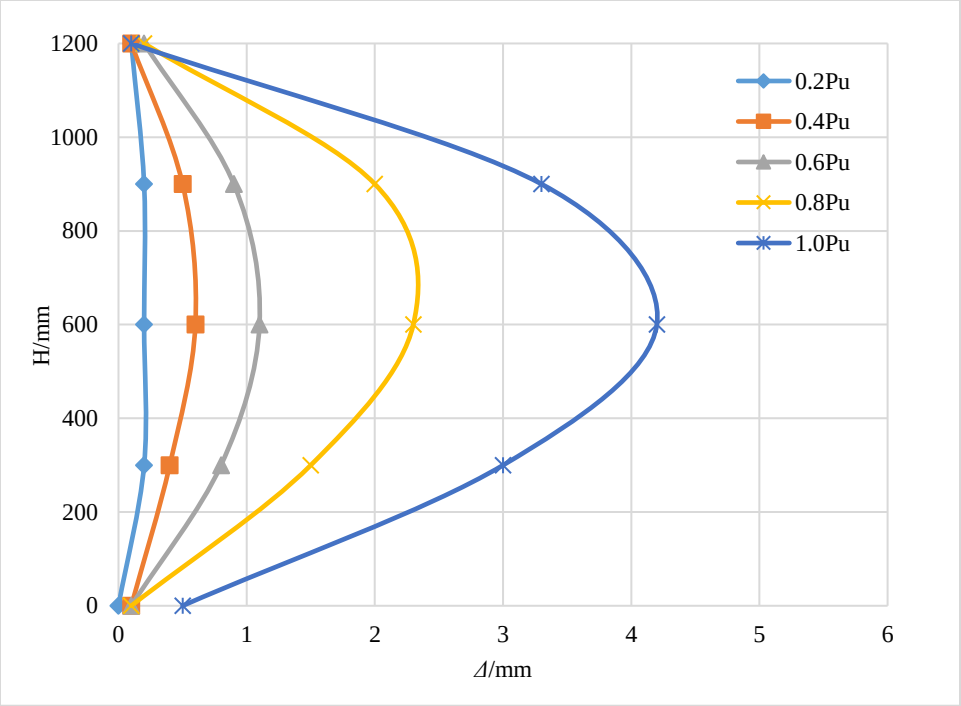
1200
1000
800
600
400
200
0
H/mm
0
1
2
3
4
5
6
Δ/mm
0.2Pu
0.4Pu
0.6Pu
0.8Pu
1.0Pu

(c) XPL-2

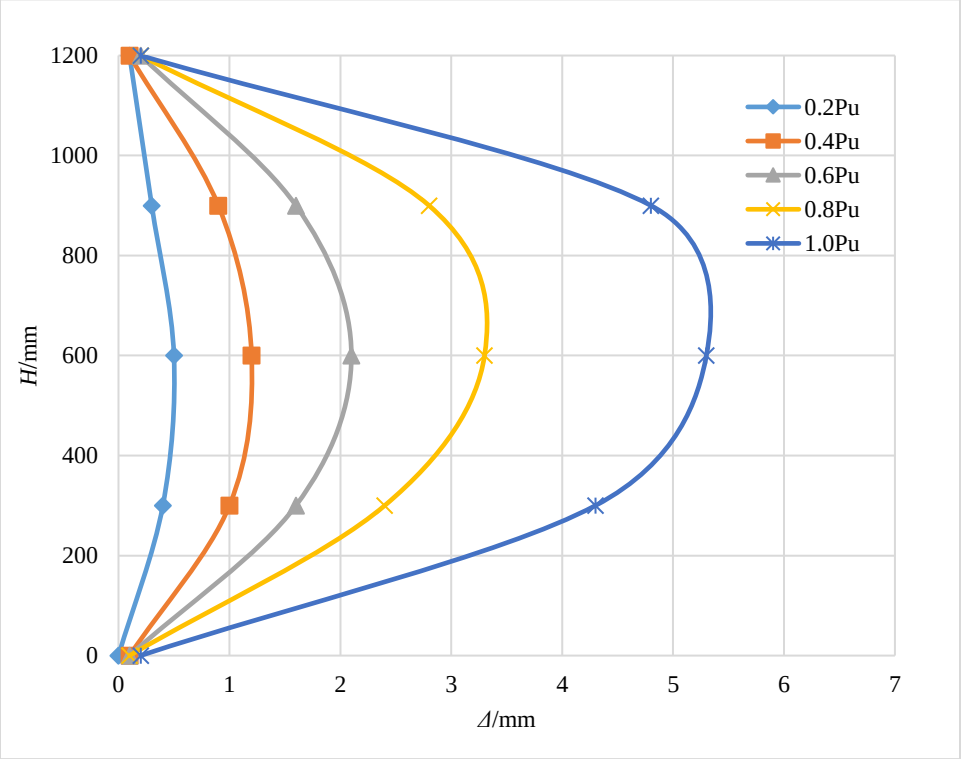
1200
1000
800
600
400
200
0
H/mm
0
1
2
3
4
5
6
7
Δ/mm
0.2Pu
0.4Pu
0.6Pu
0.8Pu
1.0Pu

(d) XPL-3

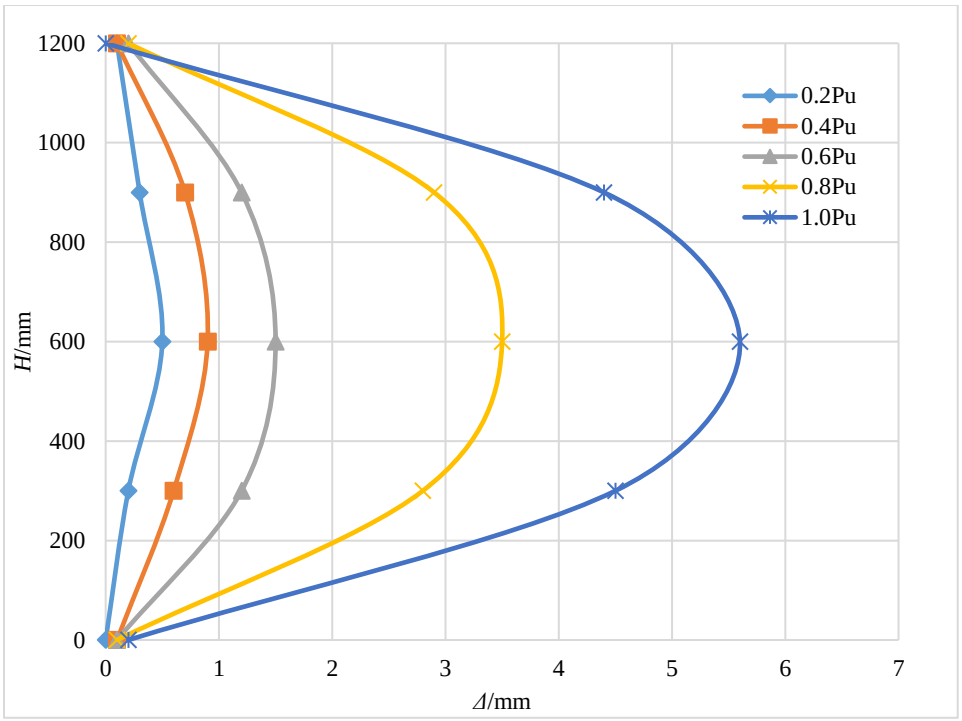
1200
1000
800
600
400
200
0
H/mm
0
1
2
3
4
5
6
7
Δ/mm
0.2Pu
0.4Pu
0.6Pu
0.8Pu
1.0Pu

(e) XPL-4

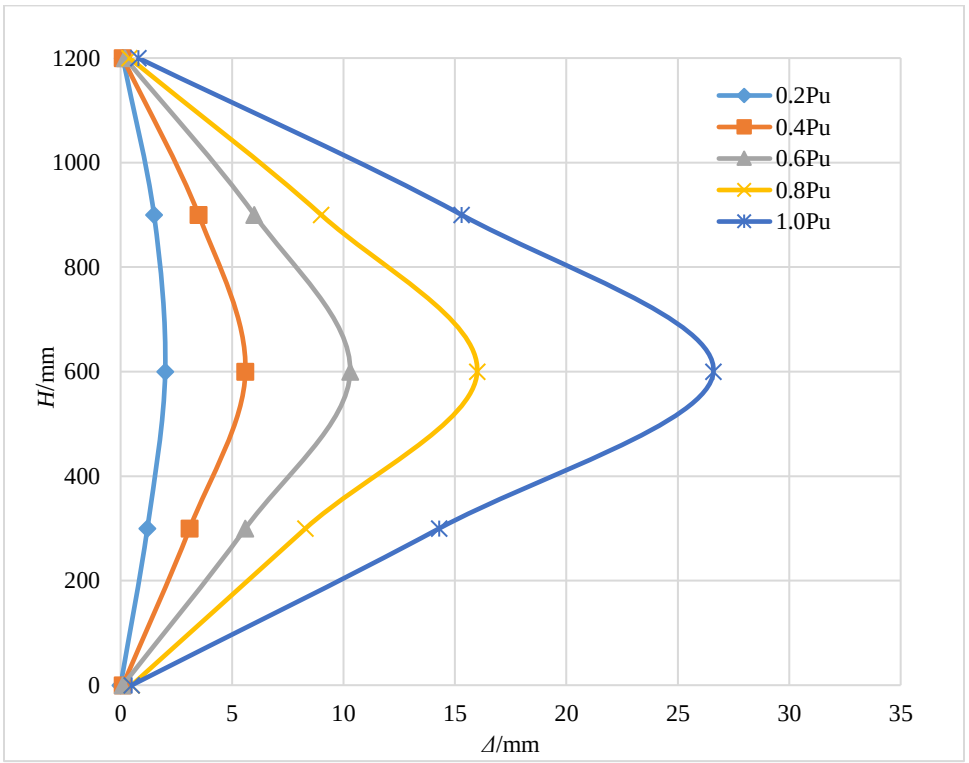
1200
1000
800
600
400
200
0
H/mm
0
5
10
15
20
25
30
35
Δ/mm
0.2Pu
0.4Pu
0.6Pu
0.8Pu
1.0Pu

(f) DPL

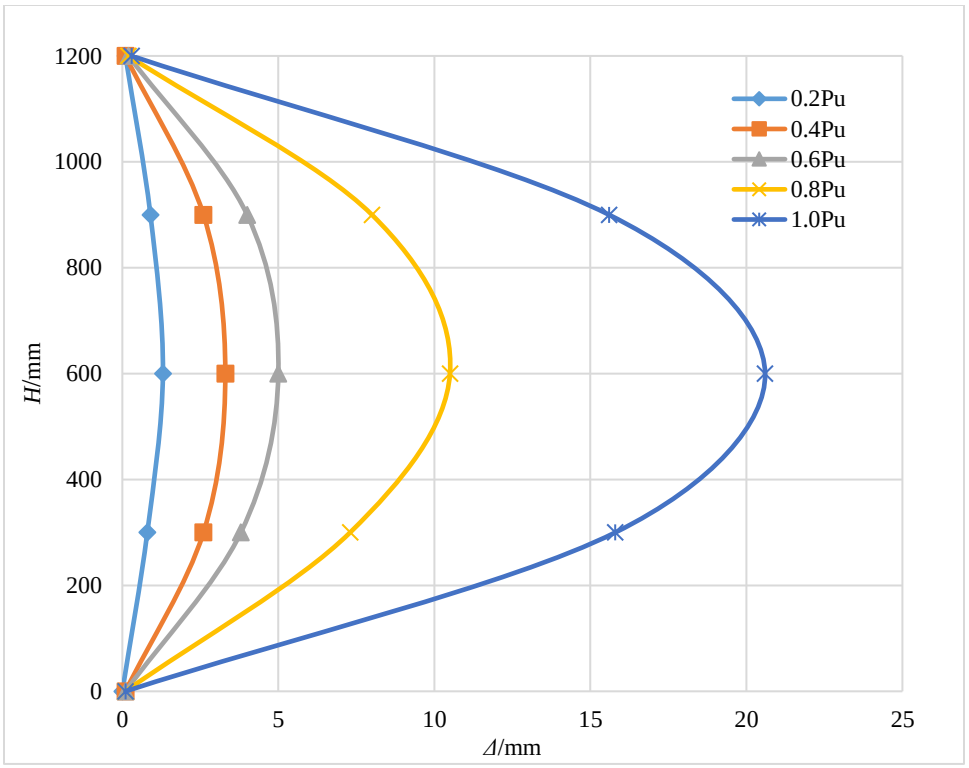
1200
1000
800
600
400
200
0
H/mm
0
5
10
15
20
25
Δ/mm
0.2Pu
0.4Pu
0.6Pu
0.8Pu
1.0Pu

(g) DPL-1

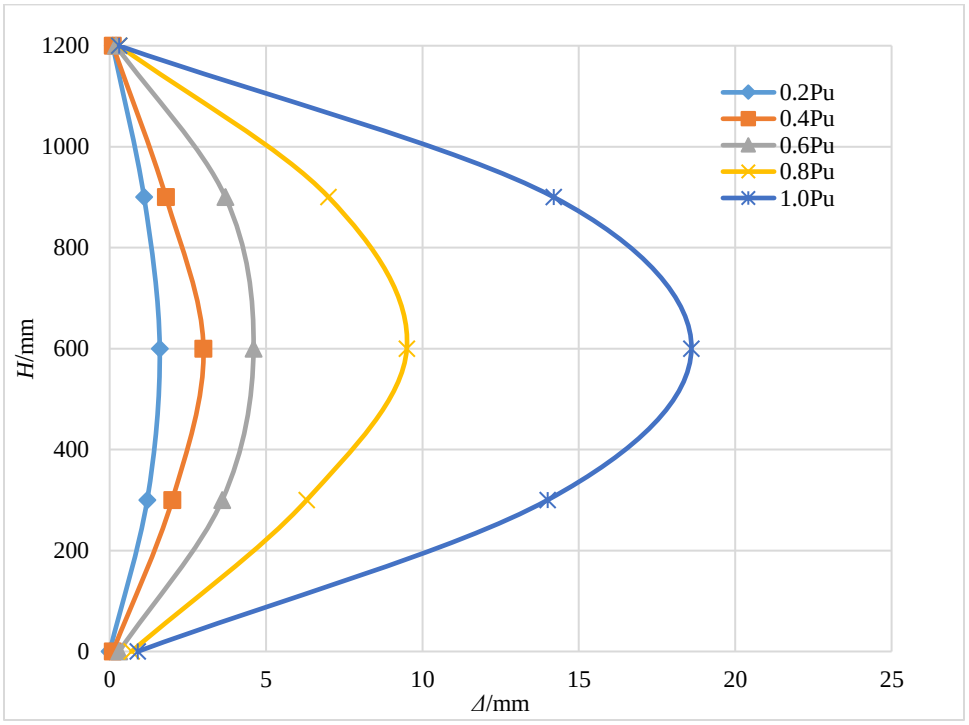
1200
1000
800
600
400
200
0
H/mm
0
5
10
15
20
25
Δ/mm
0.2Pu
0.4Pu
0.6Pu
0.8Pu
1.0Pu

(h) DPL-2

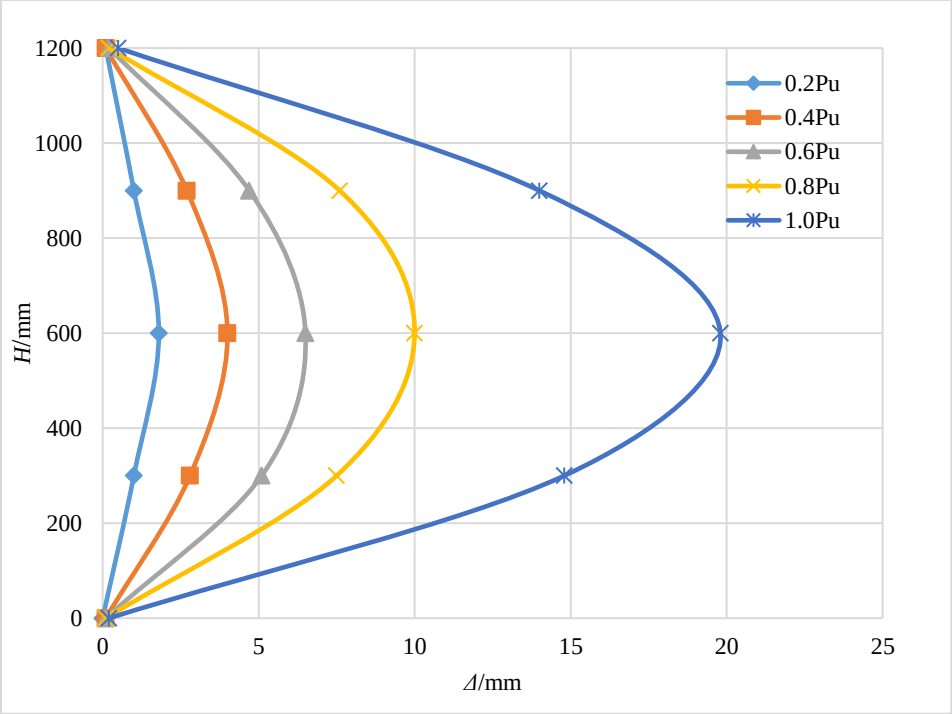

(i) DPL-3

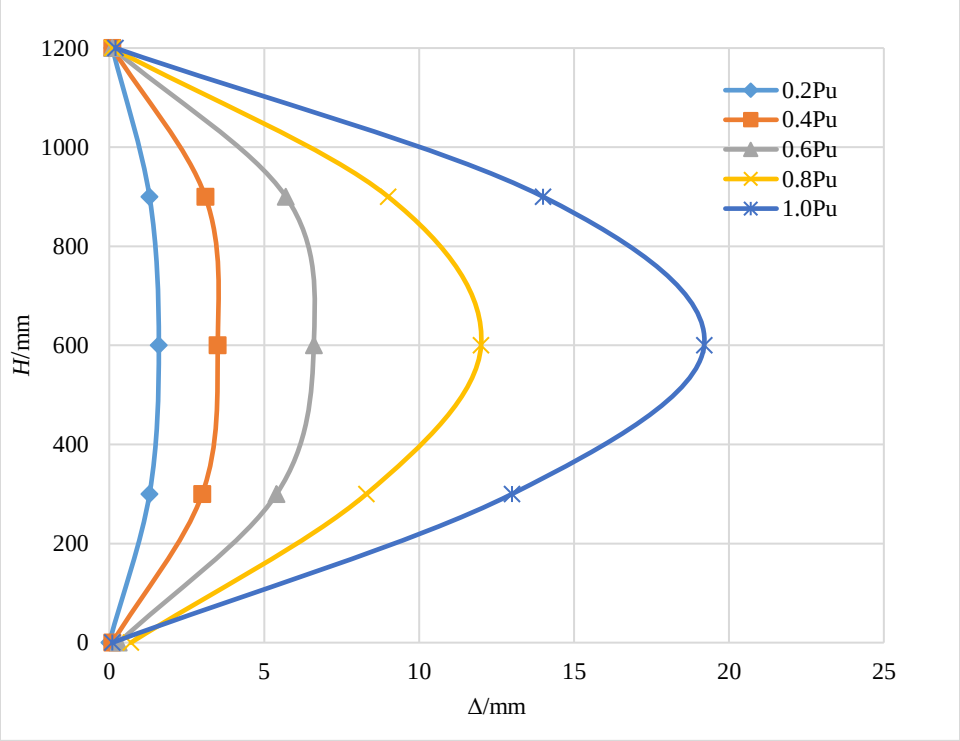

(j) DPL-4

Fig.11 deflection curve

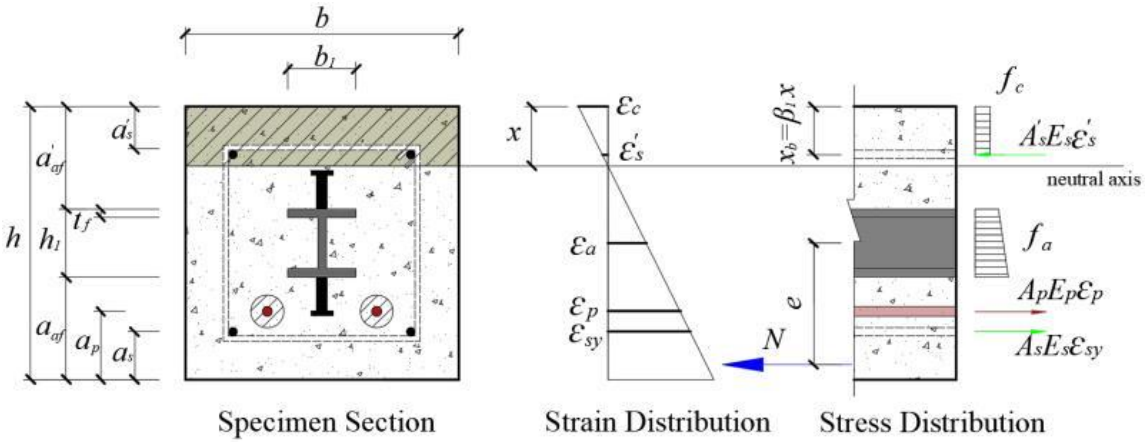

(a) the neutral axis is located inside the test section

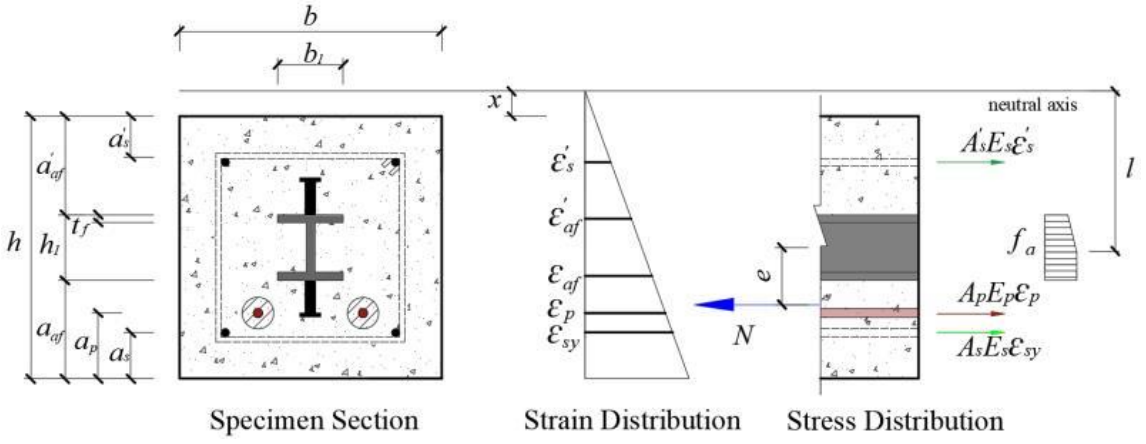

(b) the neutral axis is located outside the test section

Fig.12 Stress-strain diagram of the small eccentric tension member

1

Table.6 Experimental and theoretical results of yielding load

specimen	P_y /kN		
	Experimental value	Theoretical value	E/T
XPL	267	307	0.87
XPL-1	343	336	1.02
XPL-2	332	355	0.94
XPL-3	402	424	0.95
DPL	248	253	0.98
DPL-1	300	281	1.06
DPL-2	319	300	1.06
DPL-3	332	361	0.92
XPL-4	374	401	0.93
DPL-4	341	340	1.00

2

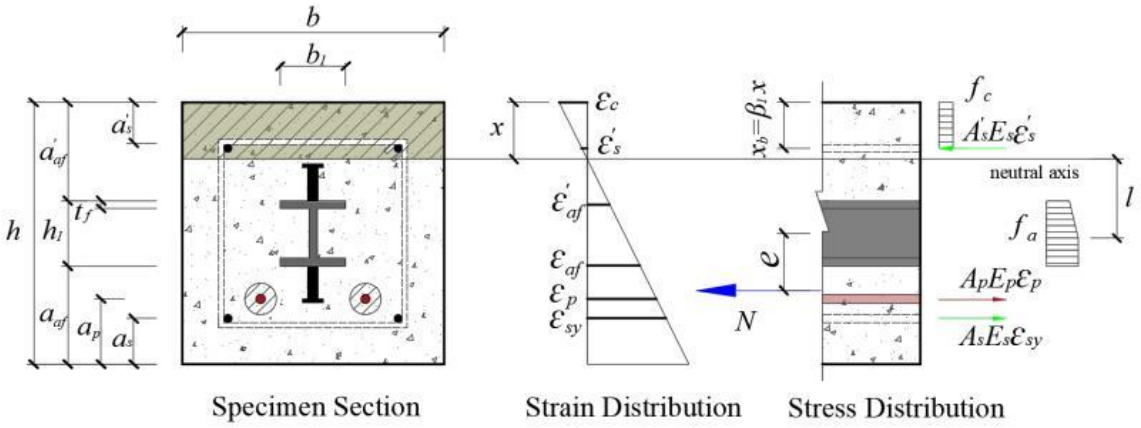

(a) the neutral axis is located outside the section of the steel

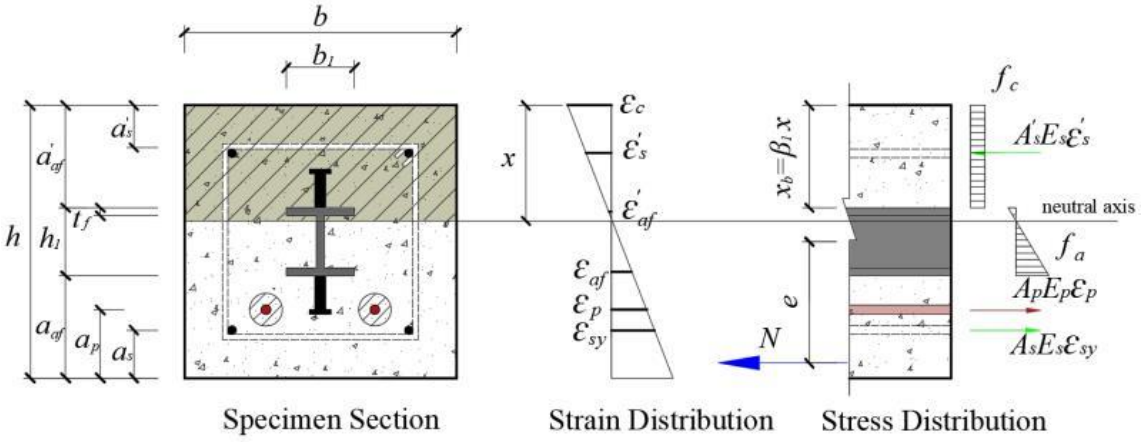

(b) the neutral axis is located inside the section of the steel

Fig.13 Stress-strain diagram of the large eccentric tension member